AD-A124 046 MECHANISMS OF SMOKE REDUCTION IN THE HIGH-PRESSURE COMBUSTION OF EMULSIFI..(U) SOUTHWEST RESEARCH INST SAN ANTONIO TX L G DODGE ET AL. DEC 82 SWR-6287/2 1/1

UNCLASSIFIED N00014-80-K-0460 F/G 21/2 NL

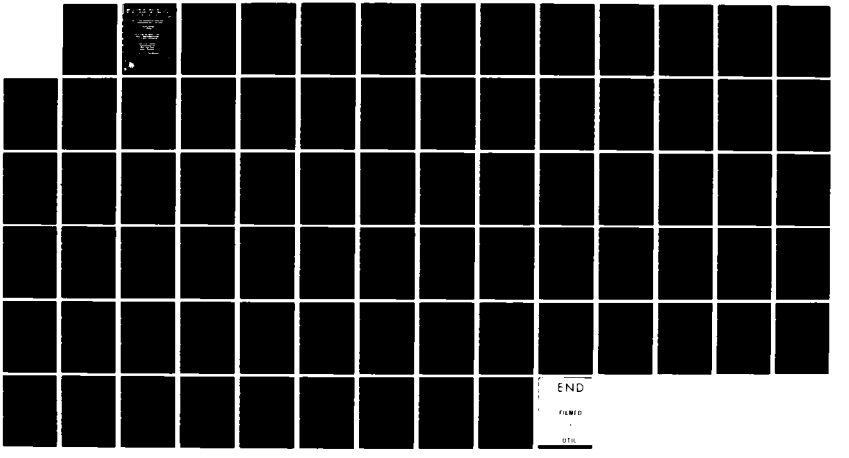

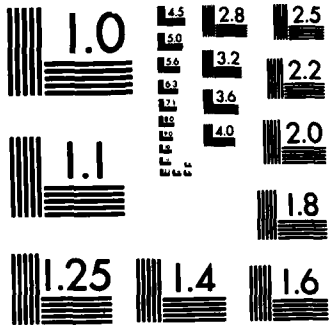


MICROCOPY RESOLUTION TEST CHART
NATIONAL BUREAU OF STANDARDS-1963-A

# TRANSIENTS OF SMOKE REDUCTION IN HIGH PRESSURE COMBUSTION OF EMULSIFIED FUELS

[redacted]



[redacted] RESEARCH INSTITUTE
[redacted] OHIO
[redacted] DIVISION

SECURITY CLASSIFICATION OF THIS PAGE *(When Data Entered)*

| REPORT DOCUMENTATION PAGE | | READ INSTRUCTIONS BEFORE COMPLETING FORM |
|---|---|---|
| 1. REPORT NUMBER | 2. GOVT ACCESSION NO. AD-A114046 | 3. RECIPIENT'S CATALOG NUMBER |
| 4. TITLE *(and Subtitle)* Mechanisms of Smoke Reduction in the High Pressure Combustion of Emulsified Fuels: Vol. II: Experimental and Theoretical Study of Evaporating Emulsified and Neat Fuel Sprays | | 5. TYPE OF REPORT & PERIOD COVERED Yearly Progress Rpt. No. 2 29 Sept 80 to 29 Sept 81<br>6. PERFORMING ORG. REPORT NUMBER Interim Rpt No. SwR-6287/2 |
| 7. AUTHOR(s) Lee G. Dodge and Clifford A. Moses | | 8. CONTRACT OR GRANT NUMBER(s) N00014-80-K-0460 |
| 9. PERFORMING ORGANIZATION NAME AND ADDRESSES Southwest Research Institute P.O. Drawer 28510 6220 Culebra Road San Antonio, Texas 78284 | | 10. PROGRAM ELEMENT, PROJECT, TASK AREA & WORK UNIT NUMBERS |
| 11. CONTROLLING OFFICE NAME AND ADDRESS Office of Naval Research Department of the Navy 800 North Quincy Street Arlington, Virginia 22217 | | 12. REPORT DATE December 1982<br>13. NUMBER OF PAGES 74 |
| 14. MONITORING AGENCY NAME & ADDRESS *(if different from Controlling Office)* | | 15. SECURITY CLASS. *(of this report)* Unclassified<br>15a. DECLASSIFICATION/DOWNGRADING SCHEDULE |

16. DISTRIBUTION STATEMENT *(of this Report)*

Approved for public release; distribution unlimited

17. DISTRIBUTION STATEMENT *(of the abstract entered in Block 20, if different from Report)*

18. SUPPLEMENTARY NOTES

19. KEY WORDS *(Continue on reverse side if necessary and identify by block number)*

| | | |
|---|---|---|
| Alternative Fuels | Drop Size Measurements | Evaporation |
| Atomization | Drop Sizing | Fuel Drops |
| Combustion | Drops | Lasers |
| Combustors | Emulsified Fuels | Measuring Instruments |

20. ABSTRACT *(Continue on reverse side if necessary and identify by block number)*

This report documents progress made during the second year of a three-year study of the atomization and evaporation characteristics of emulsified and alternative fuels at conditions typical of those found in gas turbine engines. The development of experimental techniques suitable for drop size measurements in realistic polydisperse fuel sprays in high pressure/temperature air has been the first goal of this year's program. The second

DD FORM 1 JAN 73 1473 EDITION OF 1 NOV 65 IS OBSOLETE

SECURITY CLASSIFICATION OF THIS PAGE *(When Data Entered)*

Area of interest has been the development of detailed drop models which predict the heat-up, evaporation, and trajectory of fuel sprays and the resulting size distribution parameters. In addition to these two areas, a facility was constructed during the first year of this program to allow for the containment of sprays in high pressure/temperature moving air with optical access for spray size measurements. These experimental and analytical tools have and will continue to be used to study the differences in atomization/evaporation of emulsified and neat fuels, and various other fuels of interest to the U.S. Navy.

Significant results of the second year of this study include the following. A commercial foward-angle laser light-scattering instrument has been modified to measure drop sizes in evaporating and burning sprays. Using this apparatus it has been shown that emulsified and neat fuels initially atomize to about the same drop sizes, but at elevated temperatures and pressures, both Jet-A and hexadecane emulsions evaporate in such a way so as to produce drops of significantly smaller Sauter mean diameter (SMD) than their neat fuel counterparts at the same distance from the nozzle. The difference between the emulsified and neat fuel drop sizes only appear at elevated pressures (greater than about 3-1/2 atm) for the fuels and temperatures examined. These results are consistent with those that might be expected if microexplosions were occurring in the emulsified fuels.

A computer model has been developed based on single drop heat-up and evaporation theory. Sixteen to twenty-one size classes are used to characterize the spray and the complete heat-up, evaporation, and aerodynamic interactions are included in the model. The model is incomplete in that the inhomogeneities of the spray along the line-of-sight have not yet been included. However, the steady state drop temperature has been computed and compared with the spontaneous nucleation temperature of water for a number of conditions. These calculations suggest that the steady state drop surface temperatures at conditions where differences are seen in the evaporation characteristics of the emulsified and neat fuels are somewhat below (approximately 30K) the kinetic superheat limit for water. Spontaneous nucleation is expected to occur somewhat below the superheat limit.

## TABLE OF CONTENTS

## LIST OF ILLUSTRATIONS

## LIST OF TABLES

# MECHANISMS OF SMOKE REDUCTION IN THE HIGH PRESSURE COMBUSTION OF EMULSIFIED FUELS;

## VOL. II: EXPERIMENTAL AND THEORETICAL STUDY OF EVAPORATING EMULSIFIED AND NEAT FUEL SPRAYS

## INTRODUCTION AND BACKGROUND

High quality petroleum derived fuels are not as widely available as they were in the past. Future fuels derived from petroleum and non-petroleum sources such as coal and shale-oil will tend to be lower in hydrogen content and more viscous with more residual components. These fuels will be more difficult to atomize effectively and will tend to produce more soot during combustion. The purpose of this contract is to conduct fundamental research which addresses two separate aspects of the problems associated with atomization and burning of lower quality fuels. The first aspect is the experimental study of atomization and evaporation of water/oil emulsified fuel sprays in a real combustion environment, with a specific effort to verify the proposed "microexplosion" phenomena. The second goal is to examine the atomization and evaporation of "out-of-spec" fuels which are too viscous or non-volatile to meet the standard fuel specifications for gas turbine combustion. Both of these goals required the development of experimental techniques not previously available to study drop-size distributions of fuel sprays in high pressure evaporating and combusting systems. This report covers progress made during the second year of a three year effort to study atomization in combustors.

The first aspect of the atomization problem deals with the study of emulsified fuels. It has been shown (Refs. 1 and 2) that the increased soot formation resulting from combustion of low-hydrogen-content fuels

can be somewhat offset by mixing water or alcohol with the fuel. Several theories have been offered to explain this soot-reduction phenomena. These include: (a) better atomization of the emulsified fuel due to "microexplosions" caused by superheating and violent boiling of interior water micro-droplets; (b) a change in the chemical kinetics leading to soot production due to the increased OH or the increase in H/C ratio; (c) the reduction of liquid-phase pyrolysis processes due to lower drop temperatures resulting from the lower boiling point of water; or (d) the reduction of gas-phase pyrolysis processes due to the lower flame temperature from either strictly dilution effects or other chemical processes. One of the goals of this contract was to develop techniques to verify the existence of microexplosions in real combustion systems. Microexplosions have been observed for large emulsified drops burning in quiescent atmospheres, but no direct measurements have been successfully performed on realistic sprays in turbulent air. Some of the observed microexplosion phenomena have been criticized as unrealistic for several reasons: nucleation introduced by the supporting wire; the large size of the drops (when compared with real spray size distributions); and the lack of high aerodynamic shear forces which promote internal mixing and reduce the possibilities for microexplosions and also extend the heat-up period relative to the total lifetime of the drop. The purpose of the first part of this program was to develop methods to examine the behavior of sprays of emulsified fuels in a more realistic combustion environment.

The second part of this program involves a study of the atomization and evaporation of alternative fuels, which generally will be more difficult to atomize and evaporate when compared to present-day petroleum-based fuels. Some correlations exist for predicting the change in spray quality for small variations in fuel properties, and some models have been developed for fuel spray evaporation in combustors, but experimental data are lacking to verify these models and extend them to alternative fuels. The same experimental techniques developed for the first part of the program will be used for the second part.

## EXPERIMENTAL APPARATUS

The combustor facility and test section were described in some detail in the previous yearly progress report (Ref. 3). That system was used for these tests except that the disc, which provides recirculation for flame stabilization, was replaced with a fuel nozzle alone for the evaporation tests, and a window purge was added. These modifications, as well as a brief description of the overall system are discussed below.

Unvitiated compressed air is supplied to the test cell by three compressors and a gas-fired preheater which provide up to 1.1 kg/sec at pressures ranging from 138 kPa (1.36 atm) to 1620 kPa (16.0 atm) and temperatures up to 1090 K.

The test section consists of a type 316 stainless steel pipe, 16.83 cm OD, 12.50 cm ID, 2.17 cm wall thickness, with quartz windows on each side having a clear aperture of 9.2 cm by 6.7 cm. A smooth transition section 5.5 cm long is provided on each end of the windows to reduce recirculation zones. Each window is purged by air on both top and bottom. Air is supplied to each window by a total of 10 tubes of nominal 0.635 cm OD and then diffused and exhausted by a convergent section parallel to the window surface.

For the evaporation tests, the flame stabilizing disc has been replaced by a fuel nozzle alone mounted about even with the upstream edge of the windows. The nozzle is supported with a 12.7 mm OD stainless steel tube which follows the test section centerline for a distance of about 250 cm upstream from the nozzle and then makes a right angle bend and exits from the test section. The 12.7 mm OD tube carries cooling water and a separate parallel 6.35 mm OD stainless steel tube is the water return line. Another 6.35 mm OD stainless steel tube is mounted inside the 12.7 mm water cooling tube and carries fuel to the nozzle.

Fuel temperature is regulated by controlling the water cooling temperature.

The nozzles used were simplex pressure atomizers producing a hollow cone spray. The model type was Delavan Corp. WDA 45° hollow cone with nominal flow rates of 3.79 liters/hour (1 gallons/hour) and 11.3 liters/hour (3 gallons/hour) at 862 kPa (125 psi) differential pressure using water.

The operation of the test cell is monitored with a Hewlett-Packard 9820 programmable calculator which is coupled to a 50 channel scanner. A test report including the average and statistical variation of all the important parameters is available immediately after a test. The sensing systems consist of strain-gage pressure transducers, thermocouples, and turbine flowmeters.

Drop size data were obtained with a Malvern Model 2200 Particle Sizer based on the diffraction angle produced by drops when illuminated by a beam of monochromatic, coherent, collimated light from a HeNe laser. The smaller drops diffract light at larger angles to the optical axis than the larger drops. Detection is accomplished with a 30 annular ring set of solid state detectors. Detector outputs are multiplexed and the data signal-averaged with a Commodore PET computer. A fairly complex (and proprietary to Malvern) computer routine is used to interpret the light scattering pattern of the polydisperse drop systems. The drop-size data are available as either a set of two parameters defining a Rosin-Rammler, log-normal, or normal distribution, or as a histogram of 15 size classes of drops without any assumption about the shape of the distribution. Although all of the distributions have been tried, the Rosin-Rammler has generally provided the best fit and was used throughout this program. A 300 mm focal length f/7.3 lens was used to collect the scattered light. The laser beam diameter was 9 mm with a Gaussian intensity distribution truncated at the edge by the 9 mm aperture.

Several modifications were made to the Malvern drop sizer for these measurements to avoid problems associated with flame radiation during the burning spray measurements, and laser beam steering problems during both non-burning evaporation tests and burning sprays.

Three modifications were made to discriminate against flame radiation. First the laser beam was chopped at 667 Hz and the differential signal at each detector ring was sampled for 20 cycles. This necessitated slowing the multiplexing rate in the electronics from about 1.3 ms/channel to 30 ms/channel. It was also necessary to sample only the "clean" part of the signal when the beam was completely blocked or completely transmitting as the chopper blade edge produces a large spurious signal when passing through the laser beam due to its own diffraction pattern. The second modification was the use of a 3 nm band pass interference filter centered at the HeNe laser wavelength of 632.8 nm in front of the lens on the drop sizer. All measurements were made with the 300 mm focal length lens which has a maximum effective acceptance angle of about 2.7° from the normal axis for light reaching the detector. The transmission of the filter changes less than one percent for rays at this angle or less relative to the normal axis through the filter. However, if the 100 mm or 63 mm focal length lenses (the other standard sizes) were used, the acceptance angle increases to about 8.1° or 12.8°, respectively, and wider band pass filters would be necessary. The third modification involves the use of an aperture of diameter 32 mm located about 130 mm from the lens to block radiation from the flame which is not within the scattering volume of the laser beam.

In addition to problems with flame radiation, there are substantial problems even in non-combusting sprays in high temperature air due to steering of the laser beam caused by refractive index changes in the scattering volume resulting from thermal and compositional gradients near the drops. This results in excess spurious signals on the inner detector rings, getting worse at higher evaporation rates and finally limiting, at

some distance from the nozzle, the application of this technique for drop sizing. A technique has been developed for blocking light on the inner detector rings and extrapolating values from the outer rings. Radiation data on up to eight of the thirty rings is blocked, but even this becomes insufficient at some point in the evaporation process.

The significant fuel property data are given in Table 1. The emulsions were first blended using a homogenizer, and were also continuously recirculated through an ultrasonic cavity during use to maintain a consistent blend.

Table 1. Some Properties of Fuels Used

JET A (AL-10112F)

Viscosity at 40°C 1.72 cS

Specific gravity at 60°F 0.8049

Heat of Combustion 46.904 MJ/kg

Hydrogen Content 14.15%

Flash Point: 355K

Boiling Point Distribution (GC)

| Wt% Off | Deg K |
|---|---|
| 0.1 | 436 |
| 10 | 468 |
| 20 | 484 |
| 30 | 490 |
| 40 | 494 |
| 50 | 502 |
| 60 | 506 |
| 70 | 510 |
| 80 | 518 |
| 90 | 527 |
| 99 | 548 |
| 100 | 796 |

20% $H_2O$/2% Surfactant/78% Jet A (AL-10112F)

Viscosity at 40°C 4.47 cS

Specific gravity at 60°F 0.8618

Hexadecane (95% purity)

Viscosity at 40°C 2.98 cS

Specific gravity at 60°F 0.7774

Boiling point (nominal) 560K

20% $H_2O$/2% Surfactant/78% Hexadecane

Viscosity at 40°C 5.55 cS

Specific gravity at 60°F 0.8249

## SPRAY TRAJECTORY AND EVAPORATION MODEL

A computer model based on an array of different-sized, noninteracting drops has been developed to study the heat-up, final "wet-bulb" drop temperature, evaporation rates, trajectories and resulting size distribution parameters at locations downstream from the nozzle. The trajectory part of the model should be considered as a straightforward and simple one based on an average drop path (neglecting turbulent statistical fluctuations) in a one-dimensional flow field. This corresponds to the experimental situation being studied. The thermodynamic part of the model, however, is very detailed and computes the transient heat-up and final drop temperature in greater detail than most spray models. The environment surrounding the drop is calculated based on the properties of both the fuel vapor and air rather than air alone as in some spray models. The convective effects on evaporation are included and constantly updated as the different size drops are decelerated to the air-stream velocity. The effects of temperature and pressure on air and fuel properties is included, and the steady-state "wet-bulb" temperature is iteratively calculated using the equations for the vapor pressure and temperature-dependent fuel and air properties. This model assumes uniform drop temperatures (infinite heat transfer rates within the drop) and single-component fuels.

Some spray models have predicted the change in drop-size distribution for a quiescent spray as a function of time, but results from this model show the considerable distinction between drop-size distributions as measured at a given location along the nozzle axis, at which drops arrive after different transit times (depending on diameter), as contrasted with the variation with time. For example, in this experiment, the spray initially has a higher axial velocity than the air and the small drops decelerate more rapidly than the large ones, resulting in a higher concentration in the measurement volume for the small drops and a longer time-of-arrival. These effects must be included

in any model which is intended to be used for comparison with experimentally measured changes in size distribution.

In developing a model which can be used to compare with experimental results, it is necessary to consider the interaction of the measuring device with the spray. The added weighting of the small drops due to their more rapid deceleration has been discussed. In addition, the small drops are caught up in the air stream and tend to populate the center of the spray while the large drops maintain their initial velocity longer and tend to fill the outer edges of the spray. This disparity is magnified by the fact that at the exit of a hollow-cone swirl nozzle (the type used in these tests) the majority of the fluid consists of larger drops in the outer cone of the spray, while smaller drops fill in the less dense spray in the center of the cone. Thus, it is necessary to model these inhomogeneities in size distribution through the spray and also the location, diameter, and intensity distribution of the laser beam relative to the spray. At this time, the model does account for the differert trajectories of the large and small drops, but assumes that all the spray is initially at a fixed cone angle. The drop size distribution is calculated for a complete cross section of the spray at a given axial location, without regard for the laser beam sampling volume. The model also assumes that spray breakup is complete and no secondary atomization or drop agglomeration occurs beyond some point from the nozzle exit. An initial size distribution at that point is an input to the model. Thus, the model is not applicable very close to the nozzle ( $\lesssim$ 10mm).

Results from the model are presented in the following sections, while the detailed mathematics of the model are presented in Appendix A. A general flow chart of the model is presented in Figure A-1. while a listing of the Fortran source code is given in Appendix B. Most of the model has been constructed from pieces of existing models. The thermodynamic part of the model follows closely the work of Chin and Lefebvre at Purdue University, while the aerodynamic equations for drag,

velocity, etc. are based on a model developed at the University of Sheffield by Swithenbank, Boyson, Ayers and others. (See Appendix A for detailed references.)

The capabilities of the model can probably be best understood by examining some typical output data and also comparing the model results with experimental results. Some information available from the model is shown in Table 2 which represents a spray of n-hexadecane into air at 644 K and 4.42 atm. The air velocity was assumed to be a uniform one-dimensional axial flow of 8.54 m/s, while the initial fuel velocity was 20.76 m/s at an angle of 22.5° to the axis (45° cone angle) and a fuel temperature of 311 K. The computed drop size data assuming a Rosin-Rammler distribution are shown on the top line and include the two Rosin-Rammler parameters, $\bar{x}$ and N which specify a size and a width for the distribution, and the Sauter mean diameter (SMD) which is an "average" drop size. By definition, if all drops in the spray were equal in size to the SMD, then the volume-to-surface-area ratio of the imaginary monodisperse spray would be equal to the actual spray. This ratio is chosen because surface area regulates evaporation rates while the volume indicates the quantity of fuel. The initial drop sizes are shown in column 1 and the initial relative population of drops in each size class were computed to correspond exactly to a Rosin-Rammler distribution specified as an input to the program. (Those values were $\bar{x}$ = 57 and N = 1.5 for the example shown.) Because of evaporation and the more rapid deceleration of the small drops (resulting in an increased weighting for the small drops), the size distribution changes at positions downstream from the nozzle. The drop-size distribution no longer corresponds exactly to the Rosin-Rammler distribution, and the degree to which it does fit that distribution is given by the correlation coefficient. For the cases examined, the correlation coefficient has been in excess of 0.97, but under some conditions it could be worse. These distribution parameters are calculated from information shown for individual drop size classes in the lower part of Table 2.

**Table 2. Example Output from Computer Model**

| | R-R XBAR (UM) | | | R-R N | | CORR.COEF. | | SMD | | |
|---|---|---|---|---|---|---|---|---|---|---|
| | 68.9 | | | 2.52 | | .991 | | 46.51 | | |
| Initial DIAM | DIAM | TIME | X DROP | Y DROP | Z DROP | U-VEL | V-VEL | W-VEL | FTEMP | RE |
| 5.6 | .9 | .00026 | .0074 | .0021 | 0.0000 | 8.540 | .000 | 0.000 | 520.4 | .0 |
| 7.0 | .9 | .00040 | .0088 | .0023 | 0.0000 | 8.540 | .000 | 0.000 | 520.4 | .0 |
| 8.8 | .9 | .00062 | .0110 | .0025 | 0.0000 | 8.540 | -.000 | 0.000 | 520.4 | .0 |
| 11.1 | .9 | .00095 | .0142 | .0028 | 0.0000 | 8.540 | .000 | 0.000 | 520.4 | .0 |
| 14.0 | .9 | .00145 | .0191 | .0033 | 0.0000 | 8.540 | -.000 | 0.000 | 520.4 | .0 |
| 17.6 | 1.3 | .00220 | .0264 | .0041 | 0.0000 | 8.540 | .000 | 0.000 | 520.4 | .0 |
| 22.2 | 18.6 | .00202 | .0264 | .0053 | 0.0000 | 8.658 | .088 | 0.000 | 505.6 | .3 |
| 28.0 | 27.4 | .00179 | .0264 | .0068 | 0.0000 | 9.310 | .575 | 0.000 | 460.2 | 3.1 |
| 35.2 | 35.2 | .00157 | .0264 | .0082 | 0.0000 | 10.811 | 1.696 | 0.000 | 411.3 | 12.4 |
| 44.4 | 44.4 | .00142 | .0264 | .0091 | 0.0000 | 12.708 | 3.112 | 0.000 | 377.2 | 30.7 |
| 55.9 | 55.9 | .00135 | .0265 | .0096 | 0.0000 | 14.156 | 4.193 | 0.000 | 355.5 | 54.9 |
| 70.5 | 70.5 | .00131 | .0264 | .0098 | 0.0000 | 14.913 | 4.759 | 0.000 | 341.1 | 81.2 |
| 88.8 | 88.8 | .00129 | .0265 | .0100 | 0.0000 | 15.372 | 5.101 | 0.000 | 331.6 | 112.3 |
| 111.9 | 111.9 | .00126 | .0264 | .0101 | 0.0000 | 15.830 | 5.443 | 0.000 | 325.0 | 153.6 |
| 141.0 | 141.0 | .00125 | .0265 | .0103 | 0.0000 | 16.230 | 5.742 | 0.000 | 320.7 | 206.3 |
| 177.6 | 177.6 | .00123 | .0265 | .0104 | 0.0000 | 16.617 | 6.031 | 0.000 | 317.7 | 275.2 |
| 223.8 | 223.8 | .00121 | .0264 | .0104 | 0.0000 | 16.971 | 6.295 | 0.000 | 315.6 | 363.8 |
| 282.0 | 282.0 | .00120 | .0264 | .0105 | 0.0000 | 17.276 | 6.523 | 0.000 | 314.2 | 476.6 |
| 355.2 | 355.2 | .00119 | .0264 | .0106 | 0.0000 | 17.549 | 6.727 | 0.000 | 313.2 | 620.7 |
| 447.6 | 447.6 | .00118 | .0264 | .0106 | 0.0000 | 17.790 | 6.907 | 0.000 | 312.5 | 804.3 |
| 563.9 | 563.9 | .00118 | .0265 | .0107 | 0.0000 | 17.992 | 7.057 | 0.000 | 312.1 | 1036.5 |

The initial drop sizes (in $\mu$m) are shown in column 1 while the instantaneous drop sizes are shown in column 2 at a distance from the nozzle of 26.4 mm as shown in column 4 and a time (in seconds) as specified in column 3. When the drops reach a diameter of 0.9 $\mu$m they are assumed to be completely evaporated and the diameter is fixed at 0.9 $\mu$m to keep some of the computations from becoming undefined. For those cases, the time and location are frozen at the point where the drop disappeared and those drops are not used in calculating the Rosin-Rammler parameters. Note that this model calculates spray data at a given axial distance from the nozzle (X DROP) and not at a given time from injection. The smaller drops take longer to reach the specified location due to their lower velocity as specified in column 7 by U-VEL in m/s. The smaller drops decelerate to the air stream velocity of 8.54 m/s more rapidly than the large drops. The coordinate system is cylindrical with the axial coordinate being x with velocity u, the corresponding radial components y and v, and the corresponding angular components (assumed zero presently) z and w. Distances are in meters and velocities in meters/second.

Note the difference in trajectories and velocities for the different size classes. All non-evaporated drops are at the same axial (X DROP) location but the radial location (Y DROP) of the small drops is less than the large ones due to their being caught up in the air stream sooner as shown by the axial (U-VEL) and radial (V-VEL) velocities. The wide variation in Reynolds numbers (RE) is shown in the last column. The importance of convective effects in heat and mass transfer is obvious from these values, and hence, the shortcomings inherent in quiescent spray models.

The instantaneous drop temperature (FTEMP) is shown in the next to the last column. The initial fuel temperature was 311 K and the "wet-bulb" final steady-state drop temperature is 520 K at these conditions. The normal boiling point of n-hexadecane is 560 K. Note that the small

heat up and evaporate almost instantaneously while the "uniformly mixed" temperature of the largest drops is predicted to be close to the initial fuel temperature. Due to finite rate heat transfer the surface temperature of the large drops would be higher, but experimental evidence is lacking to predict temperature profiles within the drop. Complex models have been developed to predict these profiles, but they are too cumbersome for this effort and generally lack verification.

Note the importance of modeling the transient nature of the drop before it reaches the steady-state temperature. Of the 21 drop size classes shown in Table 2, only one nonevaporated size class has reached the steady-state temperature. As the pressure and convective effects are increased, the length of the transient period relative to the steady-state period increases (Ref. 4). Thus, models that assume no mass transfer until the drop reaches its steady-state temperature are not representative of many realistic conditions in gas turbines and are insufficient to compare with experimental results generated in this program.

In addition to the drop array data just discussed, the model has been used to examine the steady-state "wet-bulb" temperature and the quiescent, evaporation rate of the fuel, which are both independent of drop size, as a function of air pressure and temperature. At atmospheric pressure, the steady-state drop temperature is lower than the normal boiling point due to the cooling effect of energy used in vaporizing the fuel. As the pressure increases, the boiling point increases and the steady-state temperature increases. Obviously the fuel and air properties are important in determining this temperature. Steady-state temperatures for three normal paraffins - octane ($C_8H_{18}$), dodecane ($C_{12}H_{26}$), and hexadecane ($C_{16}H_{34}$) - were calculated over a range of conditions with the results as shown in Figures 1 to 3. At low air temperatures, the drop temperatures converge to the air temperature. As the air temperature increases, the increased vaporization cools the drop below the air temperature, but increased pressure markedly increases the

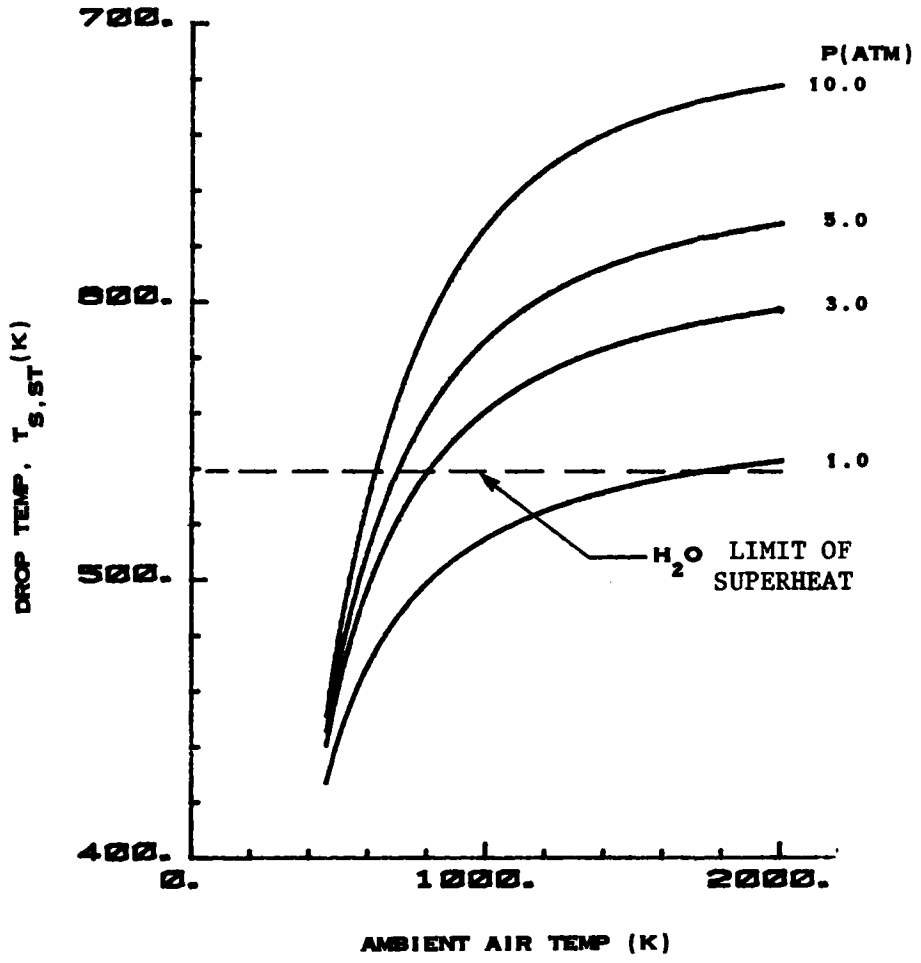


FIGURE 1. COMPUTED STEADY STATE DROP SURFACE TEMPERATURE FOR N-HEXADECANE

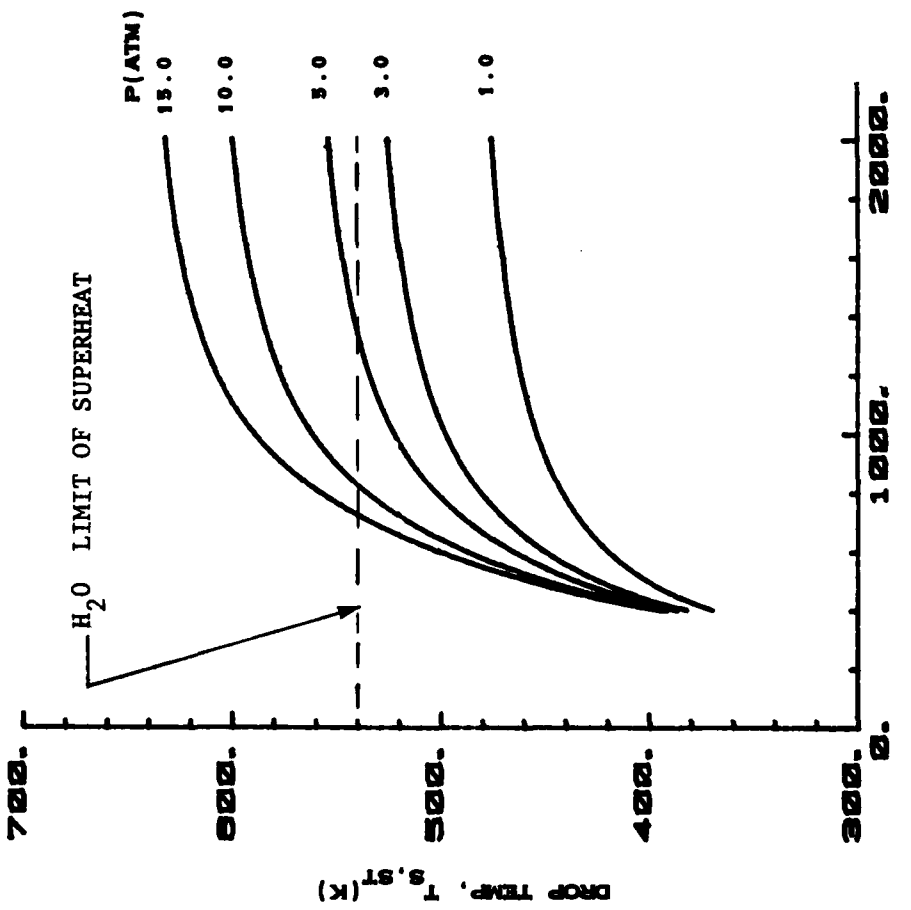


FIGURE 2. COMPUTED STEADY STATE DROP SURFACE TEMPERATURE FOR N-DODECANE

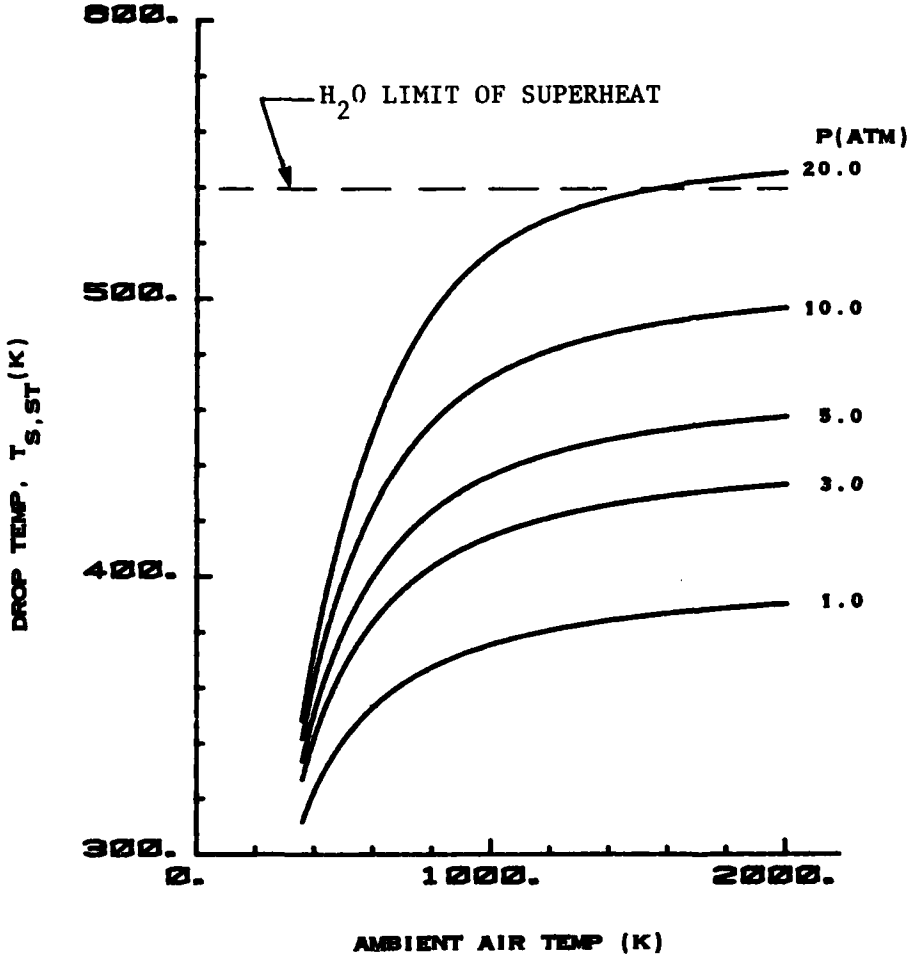


FIGURE 3. COMPUTED STEADY STATE DROP SURFACE TEMPERATURE FOR N-OCTANE

allowable drop temperature. The kinetic limit of superheat for water indicated in the figures is discussed in a later section. The critical pressure for hexadecane is 1421 kPa (14.02 atm) and for dodecane 1820 kPa (17.96 atm), and data are not shown for pressures higher than the critical pressure.

Droplet evaporation follows a D-squared law which relates the drop diameter D to the initial size $D_o$ and the time t by (Ref. 5)

$$D^2 = D_o^2 - \lambda t \tag{1}$$

where the proportionality constant $\lambda$ is the evaporation constant. The mass transfer rate of fuel from the drop, $\dot{m}_F$, at quiescent conditions is related to the evaporation constant by

$$\dot{m}_F = (\pi/4)\, \lambda \rho_F\, D \tag{2}$$

where $\rho_F$ is the fuel density. The evaporation constant is increased by convection, with a correction factor given by Frossling (Ref. 6) for cases where heat transfer rates are controlling of,

$$\lambda_{Conv.} = \lambda_{Quies.}(1 + 0.276\ Re_D^{0.5}\ Pr_g^{0.33})$$

where $Re_D$ is the Reynolds number of the gas relative to the drop and $Pr_g$ is the Prandtl number of the gas. The correction factor depends on drop size and must be calculated using the drop array part of the program, but it is instructive to examine the temperature and pressure dependence of the quiescent evaporation constant which is independent of drop size and velocity. The quiescent evaporation constants for n-octane, n-dodecane, and n-hexadecane are shown in Figures 4 to 6. It can be seen that there is a strong temperature dependence, as there must be, and a pressure dependence which is weak over the conditions used in these experiments but which increases at elevated temperatures.

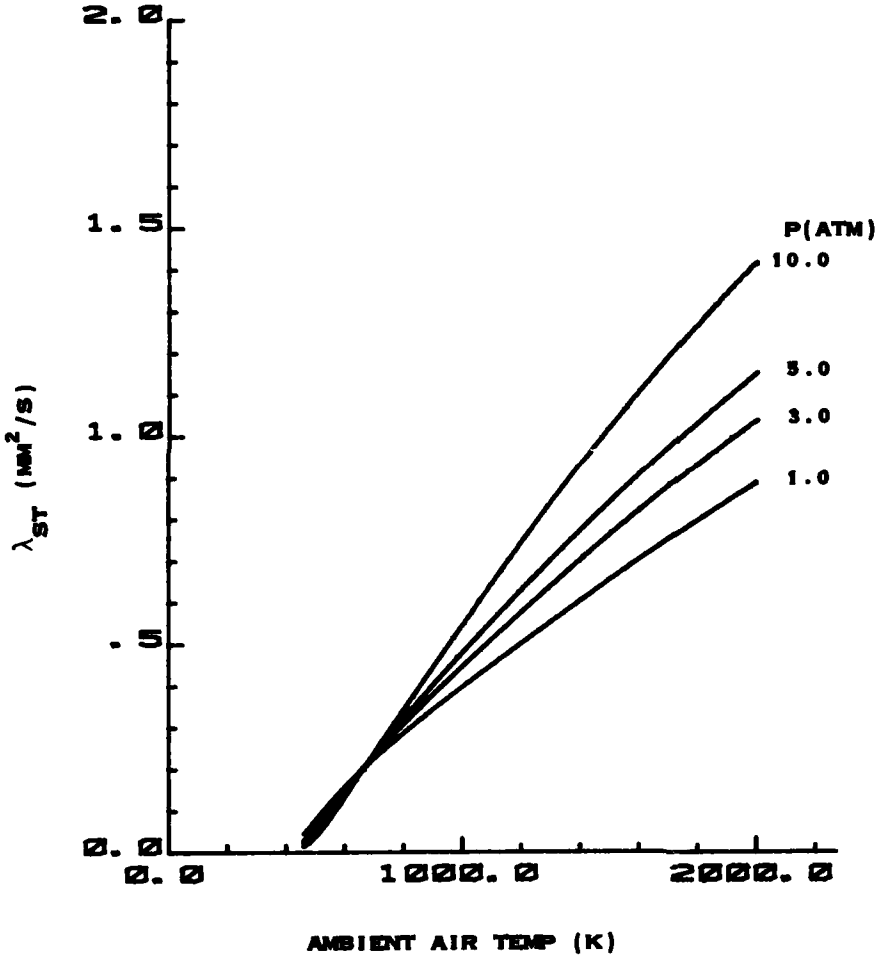


FIGURE 4. COMPUTED EVAPORATION CONSTANT AT QUIESCENT CONDITION FOR N-HEXADECANE

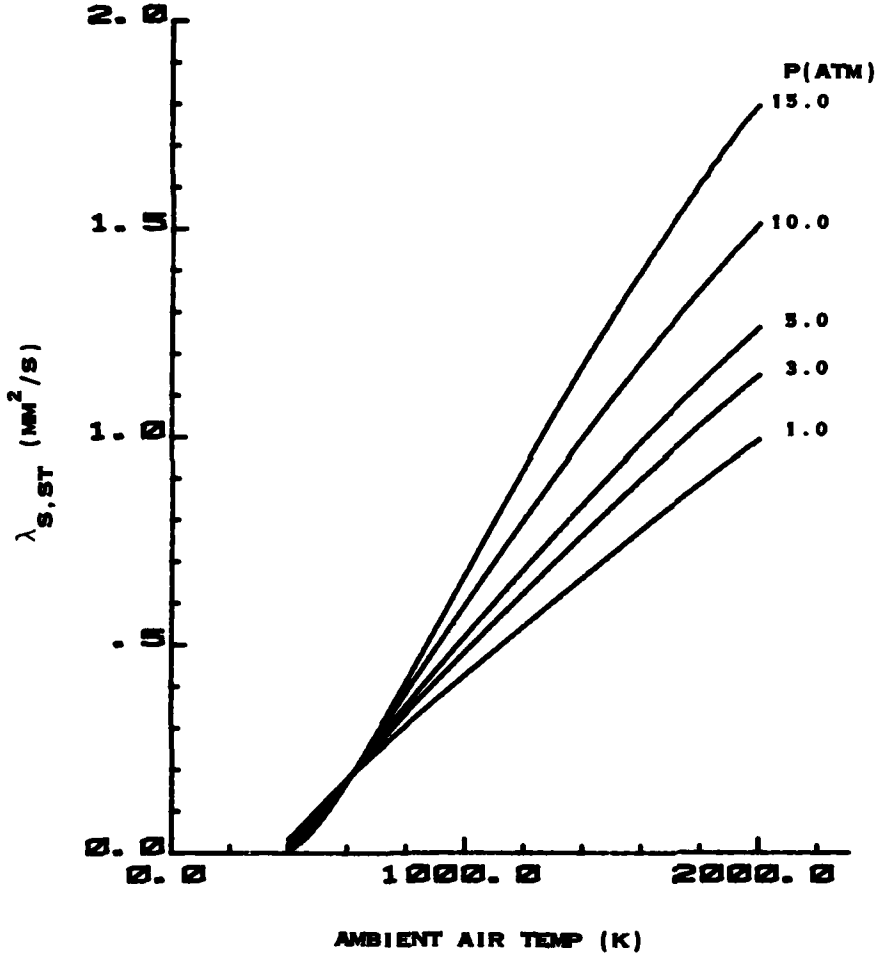


FIGURE 5. COMPUTED EVAPORATION CONSTANT AT QUIESCENT CONDITION FOR N-DODECANE

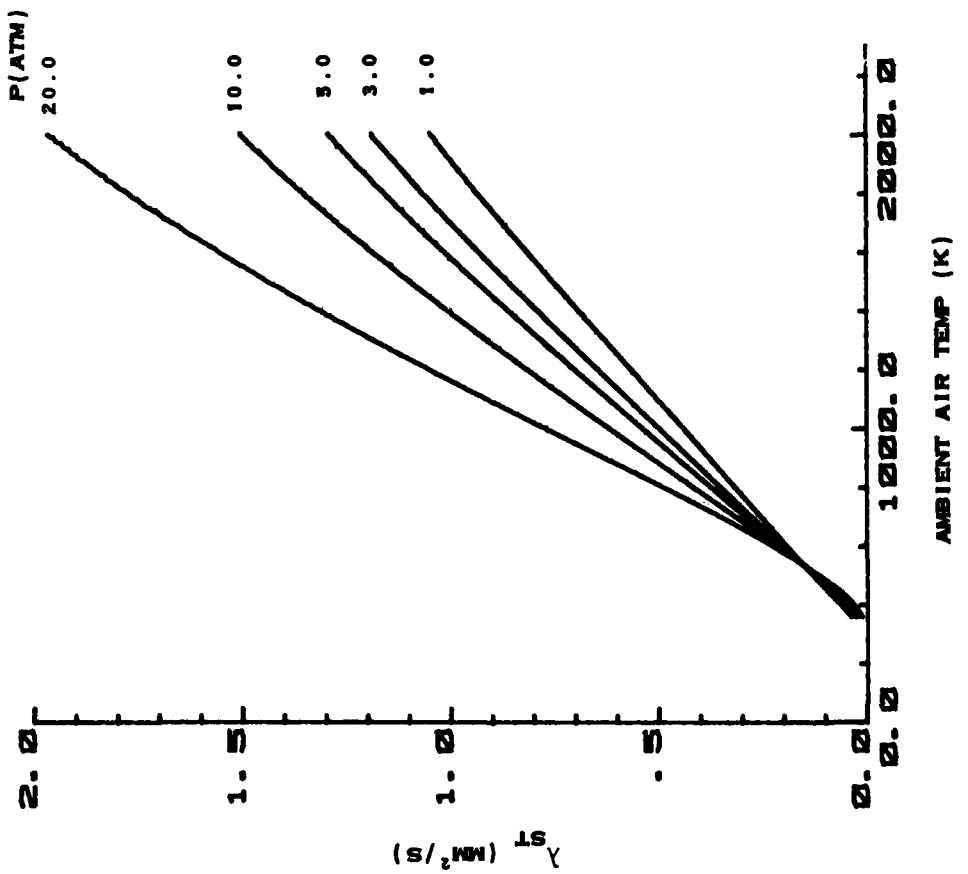


FIGURE 6. COMPUTED EVAPORATION CONSTANT AT QUIESCENT CONDITION FOR N-OCTANE

In summary, the computer model, while not completely comparable with experimental results in its present form, does provide insight into much of the thermodynamics affecting drop evaporation. It also shows quantitatively how the smaller drops are caught up in the air stream much more quickly than the larger ones. It also indicates the importance of modelling evaporation during the transient heat-up phase, particularly for realistic sprays at high pressures and Reynolds numbers. It shows the effect of air pressure on the steady-state drop temperature, and how increasing air pressure leads to increased drop temperatures which enhances the probability of initiating microexplosions.

## EXPERIMENTAL RESULTS & DISCUSSION

Experiments determining the change of drop size distribution with distance from the nozzle for emulsified and neat Jet A and n-hexadecane in high pressure/temperature flowing air have been performed. Initial experiments were performed with Jet A and showed that the emulsified fuels initially atomize to about the same size as the neat fuels and evaporate in a similar manner at low temperature and pressure conditions. However, at elevated temperatures and pressures, the emulsified fuels evaporated in such a way so as to develop smaller drop sizes than the neat fuel. Because Jet A is a multi-component fuel, as are all commercial fuels, the evaporation of even neat Jet A requires several important assumptions about the distillation process to model. For that reason, further tests were conducted with a single component fuel, n-hexadecane, and the evaporation process for a spray of that fuel has been modelled and is compared with experimental results.

The experimental results presented in this section all have the same general form consisting of graphs showing the average drop size, represented by the Sauter mean diameter (SMD), upon initial atomization close to the nozzle, and after varying amounts of evaporation moving downstream from the nozzle. In most of the plots, the SMD's were normalized near the nozzle so that the relative effects of evaporation on the emulsified and neat (without water) fuels could be seen more clearly. Each graph shows the change in average drop size as a function of distance from the nozzle for a series of air temperatures, all at a fixed air pressure, or visa versa. Data for neat fuels are shown as open symbols with solid lines drawn through the data, while data for emulsified fuels are closed symbols with dashed or dotted lines. Lines through comparable data for the emulsified and neat fuels at the same condition are called out in the figures. Drop size data are shown as close as 6.35 mm (1/4 inch) from the nozzle, in cases where the spray density was not too great, to a distance of 31.35 mm (1-1/4 inches) or

56.35 mm (2-1/4 inches) from the nozzle. Data are not shown beyond a point where excessive noise due to beam steering of the laser beam prevented reasonable results.

Atomization/Evaporation Results for Emulsified and Neat Jet A

The effects of air temperature and pressure on the atomization and evaporation of Jet A emulsions and neat fuels were examined using nominal 3.79 liter/hr (1.00 gph) and 11.4 liter/hr (3.00 gph) nozzles. Drop size data for the 11.4 liter/hr nozzle spraying into air at 310 kPa (3.06 atm) with a velocity of 14.6 m/s over a temperature range from 308 K to 644 K are shown in Figure 7. Similar data for the 3.79 liter/hr nozzle spraying into higher pressure air (448 kPa or 4.42 atm) moving at 8.5 m/s are shown in Figure 8. In Figure 8, the SMD's have been normalized so that the first point (high temperature cases) or average of first two points (lower temperatures cases) is equal to unity to show the relative evaporation more clearly. The initial average drop sizes in Figure 8 were smaller than in Figure 7 and equal to about 31 $\mu$m. (The smaller drop sizes are typical for a smaller capacity nozzle.)

These results point to a substantial difference in the evaporation characteristics of emulsified jet fuel when compared with neat jet fuel. When the air temperature is low (308 K), evaporation is relatively unimportant and microexplosions are not possible; the two fuels show a similar trend in drop-size distribution, indicated by the Sauter Mean Diameter (SMD). These data and the more extensive results presented in Ref. 3 show that the room temperature atomization characteristics of the two fuels are quite similar with the emulsified fuel usually producing slightly larger fuel drops due to the higher viscosity. This fact along with the observation that the SMD's near the nozzle tend to be approximately the same for the two fuels and diverge in moving away from the nozzle for the higher temperature cases indicate that the differences in SMD are due to differences in evaporation rather than initial

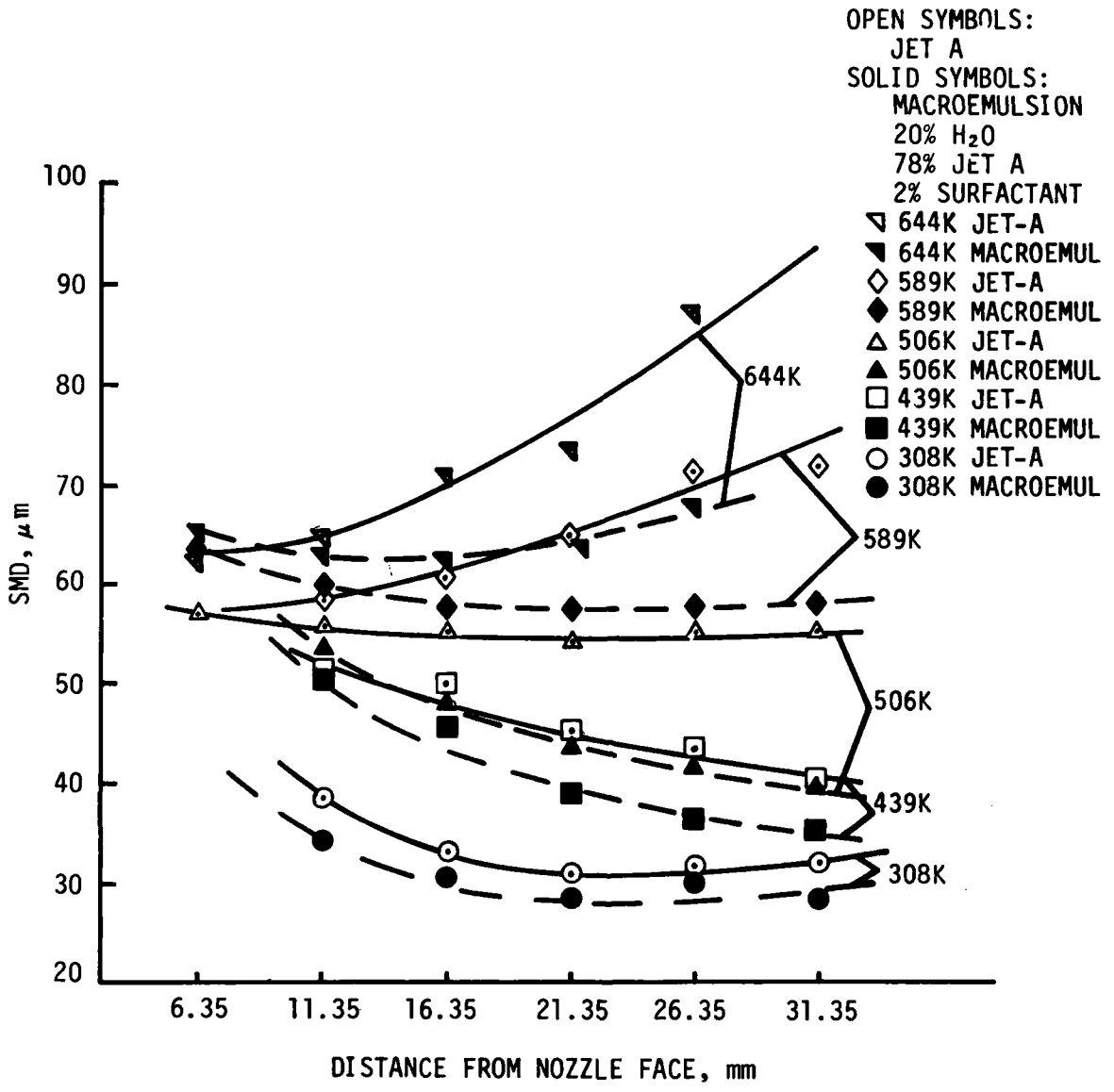


FIGURE 7. EFFECT OF AIR TEMPERATURE ON ATOMIZATION AND EVAPORATION - SMD VERSUS DISTANCE FROM NOZZLE

P = 310 kPa (∿3 atm), $V_{REF}$ = 14.6 m/S
DELAVAN 11.4 liters/hr 45° HOLLOW CONE WDA NOZZLE @ 862 kPa

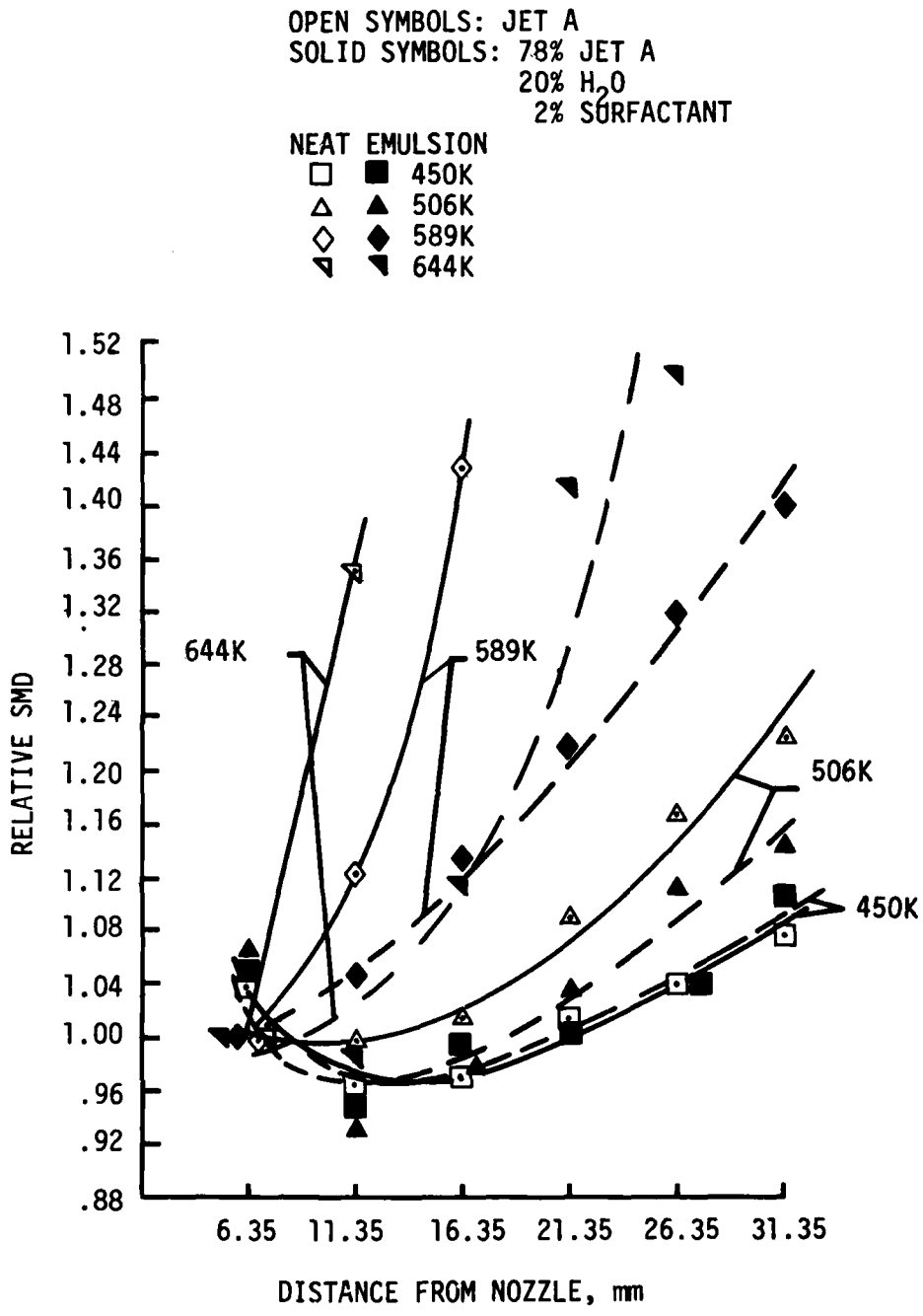


EFFECT OF AIR TEMPERATURE ON ATOMIZATION AND EVAPORATION-
RELATIVE SMD VERSUS DISTANCE FROM NOZZLE
3.8 liters/hr, 45°HC DELAVAN NOZZLE, 8.5 m/s, 448 kPa

FIGURE 8.

atomization. At elevated temperatures there is a systematic difference between two, with the emulsified fuel always showing a much lower average drop size. This is consistent with the microexplosion hypothesis, but it is necessary to diverge a bit and try to explain the general behavior of all the data in Figures 7 and 8 to better understand what other phenomena could cause the same results.

First, consider that these drop-size data were obtained with a laser-diffraction technique which measures drop characteristics along its 9 mm diameter line-of-sight, and that the measurement method can affect the results. The drop-size data in Ref. 3 for an almost nonevaporating spray in room temperature air show that the average drop size sampled by the instrument drops rapidly after leaving the nozzle, then levels out, then increases slightly. The initial reduction in SMD near the nozzle is due to at least three phenomena. First, in a hollow cone nozzle the majority of the spray volume is in the outer part of the cone composed of relatively larger drops, while a smaller amount of spray made up of smaller drops fills in the inner core. Near the nozzle the laser beam intercepts more of the outer cone increasing the average drop size. Secondly, secondary atomization may occur after the initial breakup which further reduces the large drops as distance from the nozzle increases. Third, for cases where the air velocity is lower than the initial fuel velocity as in Figures 7 and 8 and Ref. 3, the small drops rapidly decelerate to the air velocity increasing their relative concentration in the sample volume and decreasing the SMD. The differences in the drag effects on large and small drops were shown dramatically in the results of the computer model presented earlier. These three factors contribute to the decrease in SMD when moving away from the nozzle for the room temperature case where evaporation is negligible.

Now consider the elevated temperature data in Figures 7 and 8 which indicate an increase in SMD as the temperature is raised and the evaporation rate increased. This result is due to the fact that although

all drops decrease in size with evaporation, the smaller drops evaporate much more quickly and the resulting average drop size actually increases. Thus at higher air temperatures the SMD increases in moving away from the nozzle relative to the room temperature case. This is demonstrated qualitatively by results from the computer model. Data in Figures 7 and 8 show only initial trends in the change in SMD relative to the total spray lifetime. The computer model predicts and some of the data indicate that the SMD initially increases and then levels out further into the evaporation process. Also the largest SMD's shown are, in some cases, biased on the high side due to uncorrectable beam steering problems. This study is directed at the relative evaporation characteristics of emulsified versus neat fuels and the largest SMD's reported may be erroneously high.

Having qualitatively examined the phenomena responsible for the trends shown for neat Jet-A in Figures 7 and 8, it is possible to consider the reasons for the differences between the emulsified and neat jet fuel. Since the two fuels show a similar SMD near the nozzle and then the emulsified fuel shows a smaller SMD away from the nozzle, it is entertaining to speculate that microexplosions are occurring after the emulsified drops heat up and cause the larger drops to subdivide into smaller drops. However, the heat of vaporization of water is about eight items that of Jet A and the heat capacity of water is also higher so that the water may be absorbing much of the thermal energy available and reducing the evaporation rate of the emulsified fuel so that the rate of increase in drop size is reduced. This effect must be balanced against the lower boiling point of water which would tend to increase its evaporation rate. An analysis of this effect will be performed using the computer model modified to handle two fuel components.

Further tests were performed with emulsified and neat Jet A at constant air temperature with varying air pressure. Law (Ref. 7) has suggested that an increase in air pressure at constant temperature should

favor the occurrence of microexplosions because the steady state drop temperature increases with air pressure as was shown in Figures 1 to 3. The limit of superheat of water, also shown in Figures 1 to 3, is one of the criteria used to predict the condition for the onset of microexplosions. Spontaneous nucleation occurs below or at the limit of superheat (about 88 to 90 percent of the critical temperature) above which fluids will always film boil. Many liquids may be heated well above their "boiling points" and close to their predicted limit of superheat where they boil explosively. The details of the interface between the fluid and its surroundings usually determine where the fluid begins to boil in the range between the boiling point and the limit of superheat. Several investigators have chosen different temperatures to represent the condition for vaporization of the water and drop disruption; Birchley and Riley (Ref. 8) have chosen the normal boiling point, Jacques (Ref. 9) and Gollahalli (Ref. 10) use that temperature where surface tension forces are exceeded by the forces due to the internal pressure of the drop, and Law (Ref. 7) assumes drop disruption occurs at the limit of superheat. Measured values for spontaneous nucleation of water have been reported by Avedisian (Ref. 11).

Thus, although there is disagreement about the drop temperature where microexplosions occur, a higher drop temperature, as allowed by an increase in air pressure, should favor a divergence in drop sizes for emulsified and neat fuels if drop disruptions are occurring. In order to examine this possibility, tests were performed at 589 K at pressures of 207 kPa (2.04 atm) and 310 kPa (3.06 atm) with the 11.4 liter/hr nozzle, and at 547 K with pressures from 165 kPa (1.63 atm) to 448 kPa (4.42 atm) for the 3.79 liter/hr nozzle, as shown in Figures 9 and 10, respectively. These results suggest that the emulsified and neat fuels evaporate in a similar manner at the lower pressures but tend to diverge as the air pressure is increased with the emulsified fuels producing smaller drops than the neat fuels, consistent with the microexplosion hypothesis.

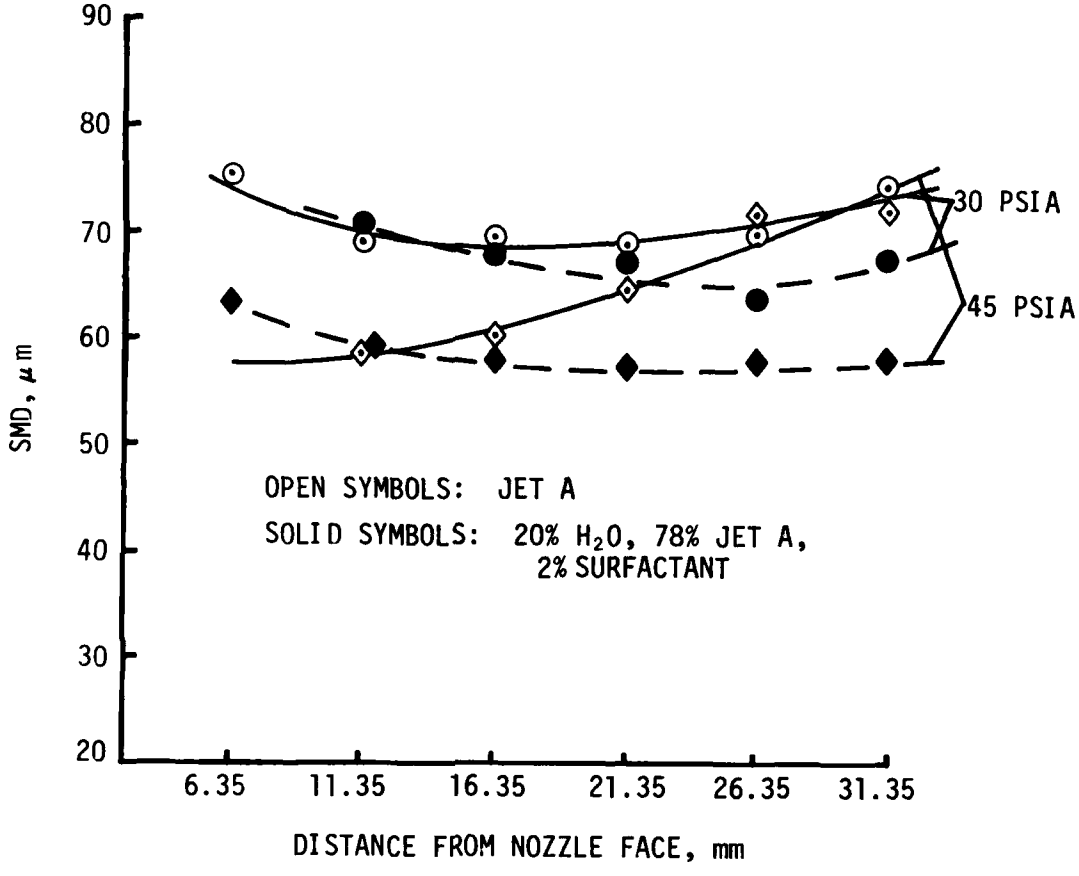


FIGURE 9. EFFECT OF AIR PRESSURE ON ATOMIZATION AND EVAPORATION - SMD VERSUS DISTANCE FROM NOZZLE ($T_{AIR}$ = 589 K, $V_{REF}$ = 14.6 m/SEC)

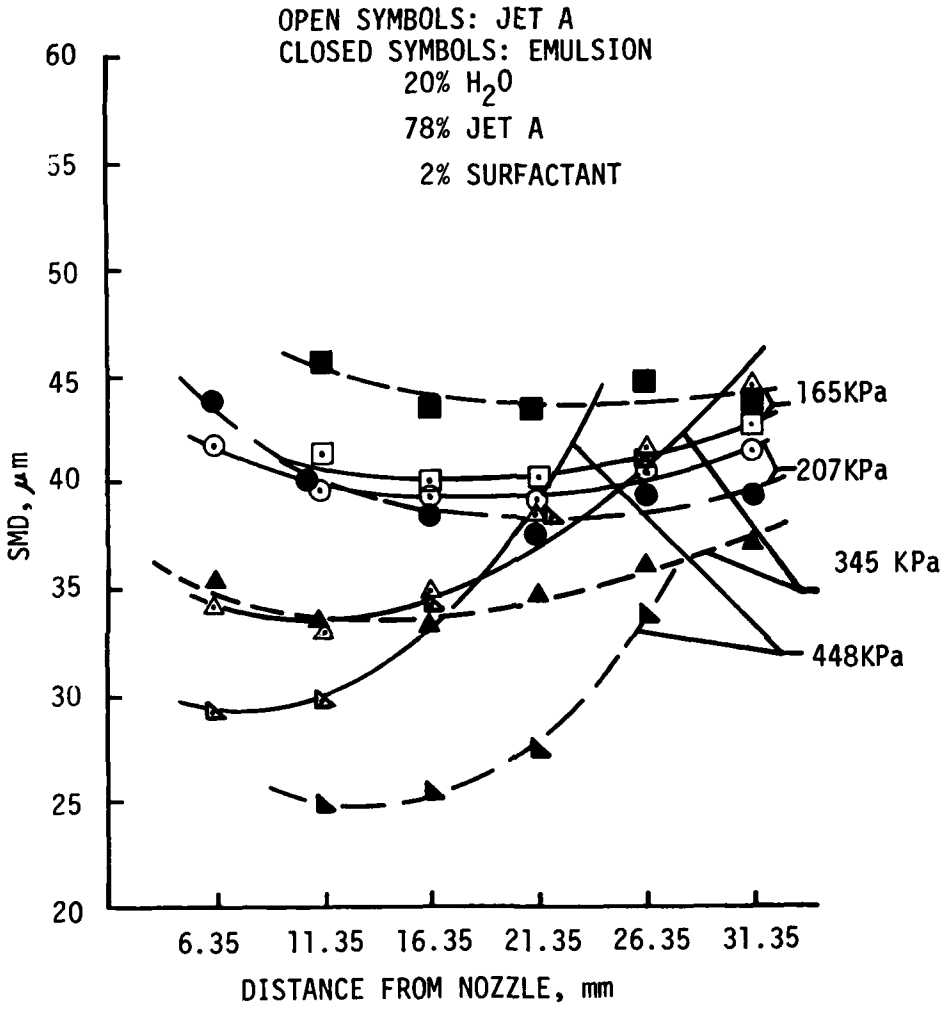


EFFECT OF AIR PRESSURE ON ATOMIZATION AND VAPORIZATION-
SMD VERSUS DISTANCE FROM NOZZLE

3.8 liters/hr 45°HC DELAVAN NOZZLE, 8.5 m/s, 547K

FIGURE 10

As an aside to the comparison of neat and emulsified fuel evaporation, consider the effect of pressure on the evaporation of neat fuel. Figures 4 through 6 indicate that the evaporation constant at quiescent conditions is approximately independent of air pressure at temperatures used in these experiments, while Figures 9 and 10 show that neat fuels evaporate faster as the pressure is increased (assuming that evaporation rates can be inferred from the rate of initial increase in SMD). This contradiction can be partly explained by three factors. First, as the air pressure increases the initial SMD decreases by a factor proportional to about $P^{-0.4}$, and the smaller drops evaporate much faster according to the $d^2$-law. Secondly, the computations in Figures 4 through 6 are for the quiescent evaporation constant while Eq. 3 shows that the convective evaporation constant depends on pressure through the Reynolds number. Third, the transit times for the drops to a fixed measurement location increase slightly with pressure due to increased drag at higher pressures, allowing more time for evaporation.

## Atomization/Evaporation Results for Emulsified and Neat Hexadecane

In order to make these arguments more quantitative, it was necessary to repeat the previous experiments with a single component fuel whose evaporation process could be modelled with greater certainty. Three single component fuels were obtained: n-hexadecane, n-dodecane, and n-octane, but experiments have been performed only with the n-hexadecane at this time. The evaporation of hexadecane drops was investigated at fixed air pressure and varying air temperature and visa versa. At a fixed pressure of 4.42 atm (448 kPa) the Sauter mean diameter (SMD) of the spray varied with distance from the nozzle as shown in Figure 11. A comparison of the size distribution of emulsified and neat fuels at 506 K and 547 K indicates no difference within the precision of the measurement. (Data for the emulsion at 506 K were essentially identical with those for the emulsion at 547 K and were omitted in Figure 11.) At 589 K the emulsified fuel produces smaller drops and the difference

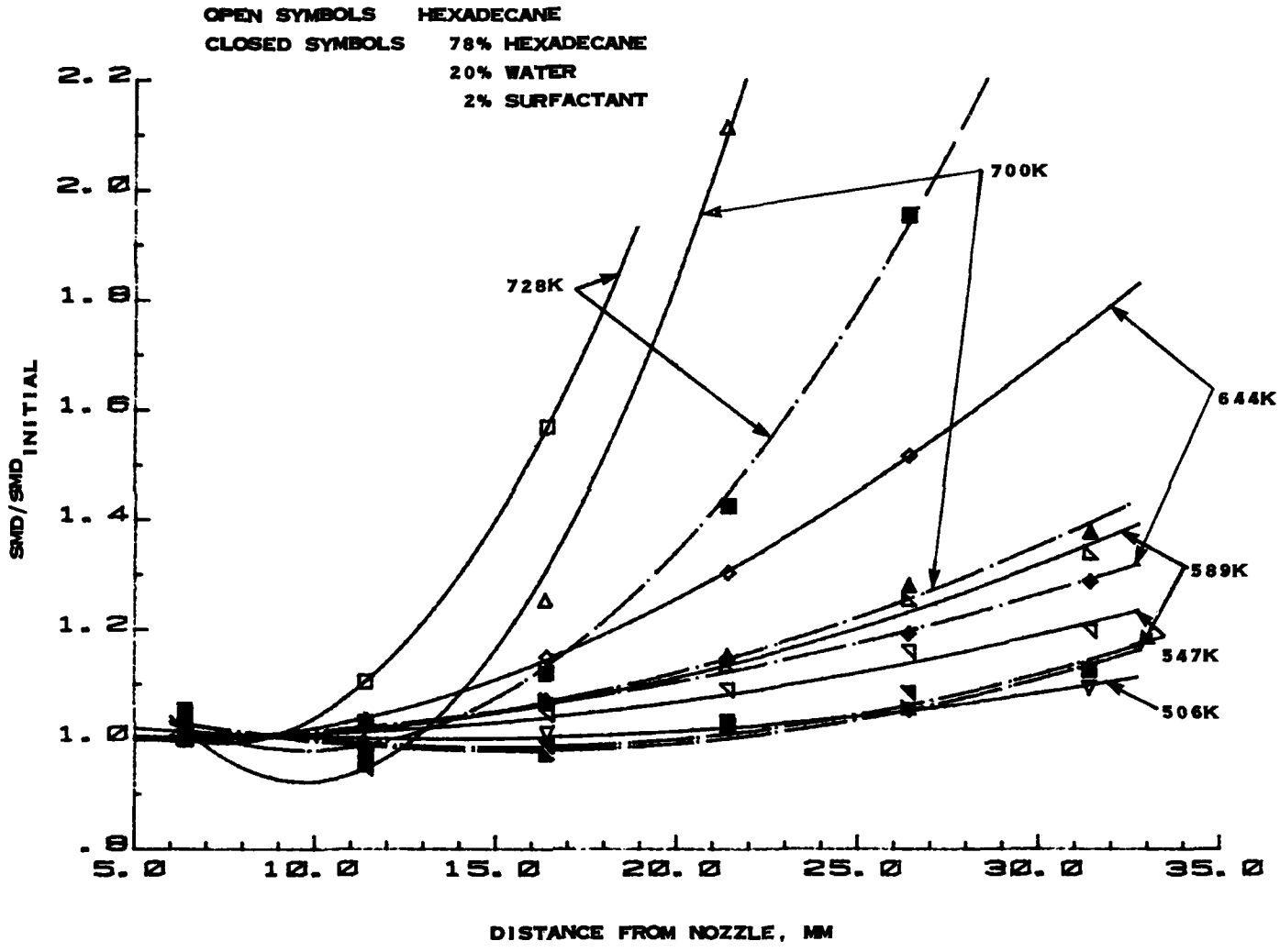


FIGURE 11. COMPARISON OF RELATIVE SMD FOR EMULSIFIED AND NEAT HEXADECANE AT CONSTANT PRESSURE (4.42 atm, 448 kPa) AND VARIOUS TEMPERATURES (DELAVAN WDA 3.8 LITERS/HR 45° HOLLOW CONE, $\Delta P$=483 kPa). $SMD_{initial} \cong 2\mu m$

increases at the higher temperatures. The corresponding predicted maximum steady-state surface temperatures of the drops as computed by the model are shown in Table 3. At a fixed temperature of 644 K the drop sizes of neat and emulsified fuels were studied as a function of air pressure with the results as shown in Figures 12-14. Examination of Figure 14 indicates that at the lower pressures of 165 kPa (1.63 atm), 241 kPa (2.38 atm), and 345 kPa (3.40 atm), the drop sizes in sprays of neat and emulsified fuels are about the same, but that at higher pressures the sprays of emulsified fuels have smaller SMD's during the heat up and evaporation process. Table 4 presents the computed droplet temperatures for these experiments.

**Table 3. Computer Predicted Steady State Drop Surface Temperatures for Hexadecane at Conditions Corresponding to Figure 11 ($P_{air}$ = 448 kPa (4.42 atm))**

| Air Temperature (K) | Drop Temperature (K) |
|---|---|
| 506 | 488 |
| 547 | 503 |
| 589 | 520 |
| 644 | 535 |
| 700 | 541 |

**Table 4. Computer Predicted Steady State Drop Surface Temperature for Hexadecane at Conditions Corresponding to Figures 12-14 ($T_{air}$ = 644 K)**

| Air Pressure (kPa) | Air Pressure (atm) | Drop Temperature (K) |
|---|---|---|
| 165 | 1.63 | 491 |
| 241 | 2.38 | 502 |
| 345 | 3.40 | 512 |
| 448 | 4.42 | 520 |
| 586 | 5.78 | 529 |

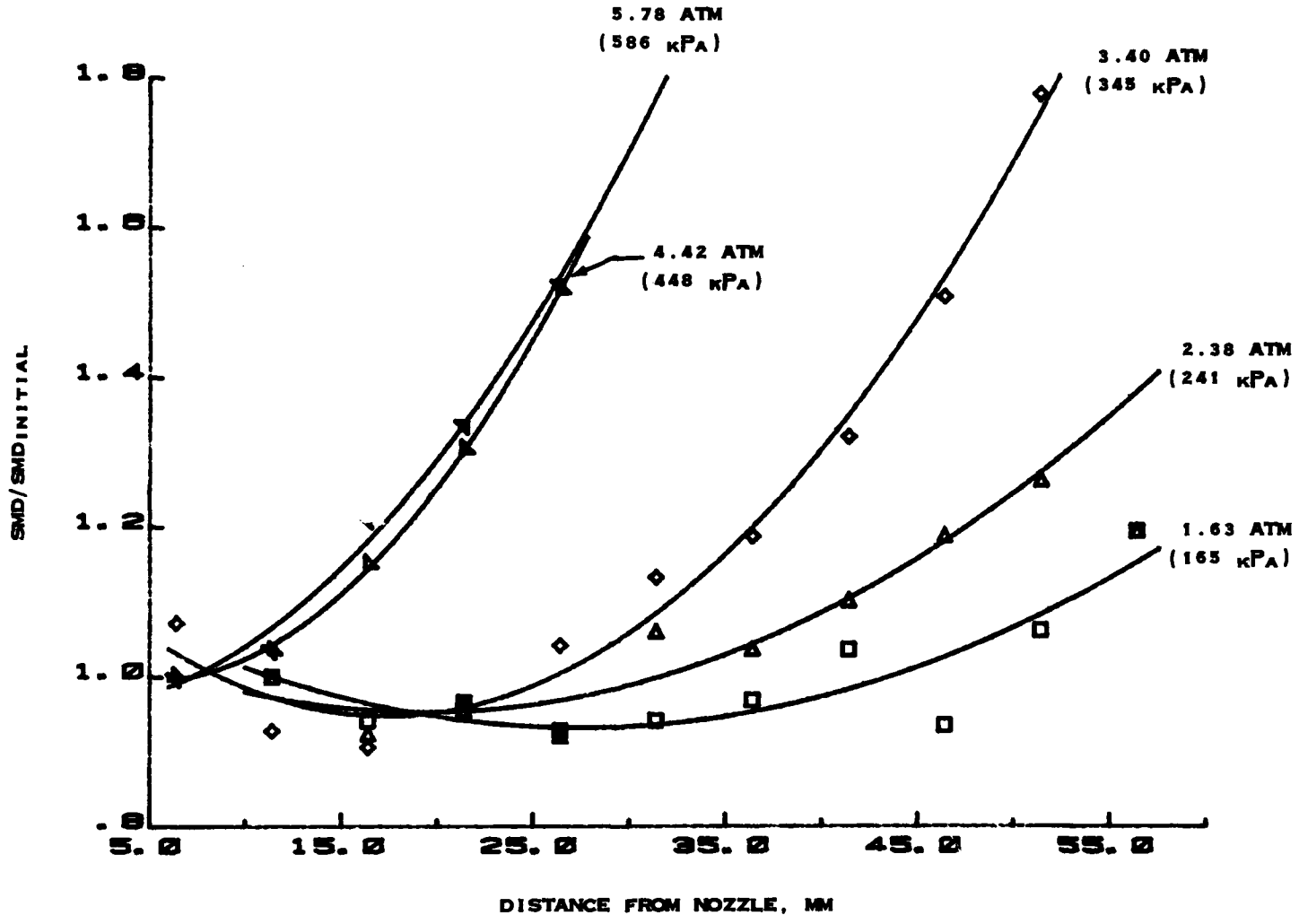


FIGURE 12. RELATIVE SMD FOR NEAT HEXADECANE AT FIXED TEMPERATURE (644K) AT VARIOUS PRESSURES (DELAVAN WDA 3.8 LITERS/HR 45° HOLLOW CONE, $\Delta P$ = 483 kPa). $SMD_{initial} \simeq 152\ P_{air}\ (kPa)^{-.250}$

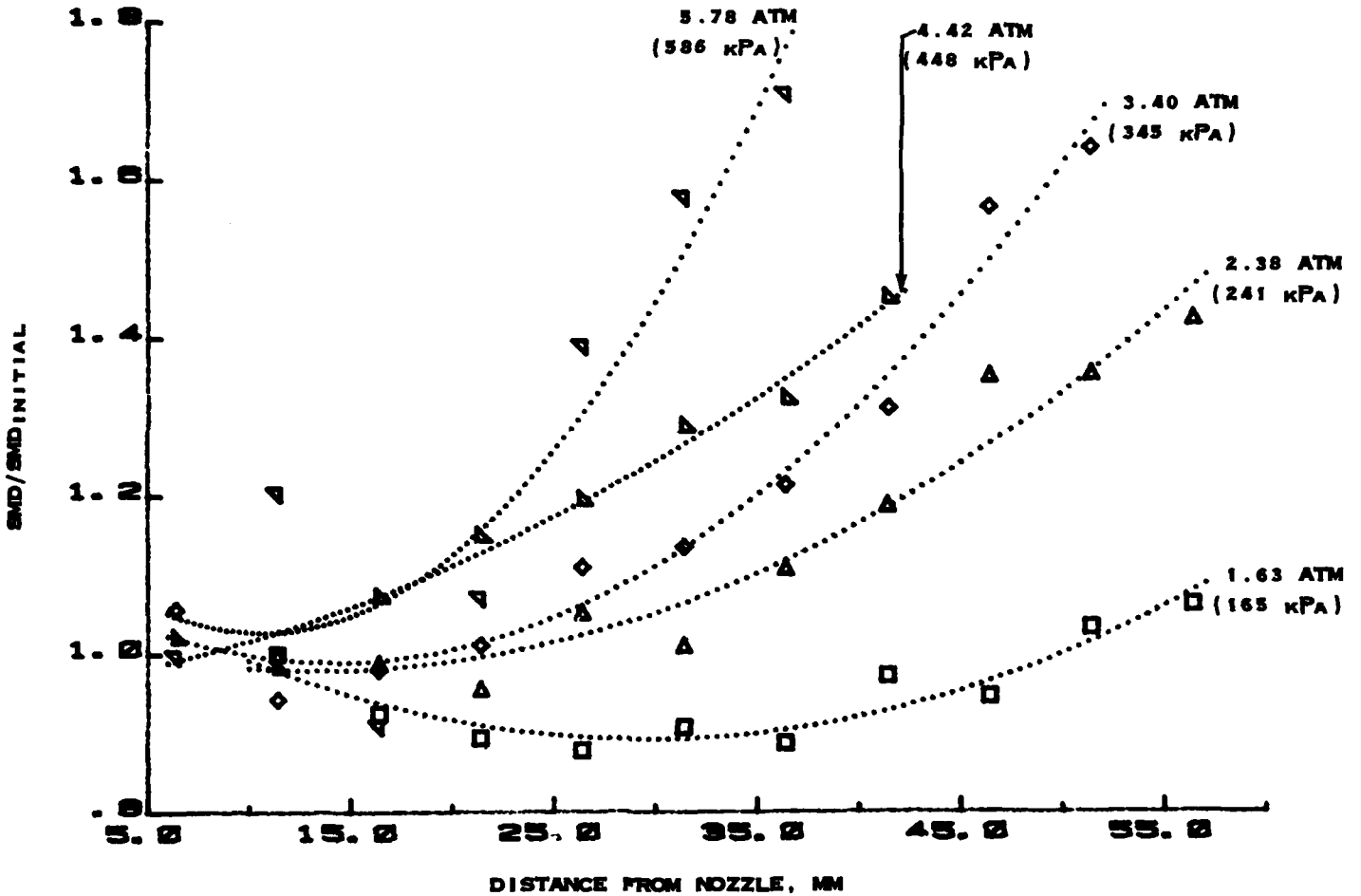


FIGURE 13. RELATIVE SMD FOR EMULSIFIED HEXADECANE AT FIXED TEMPERATURE (644K) AT VARIOUS PRESSURES (DELAVAN WDA 3.8 LITERS/HR, 45° HOLLOW CONE $\Delta P$ = 483 kPa). $SMD_{initial} \cong 152\ P_{air}\ (kPa)^{-.250}$

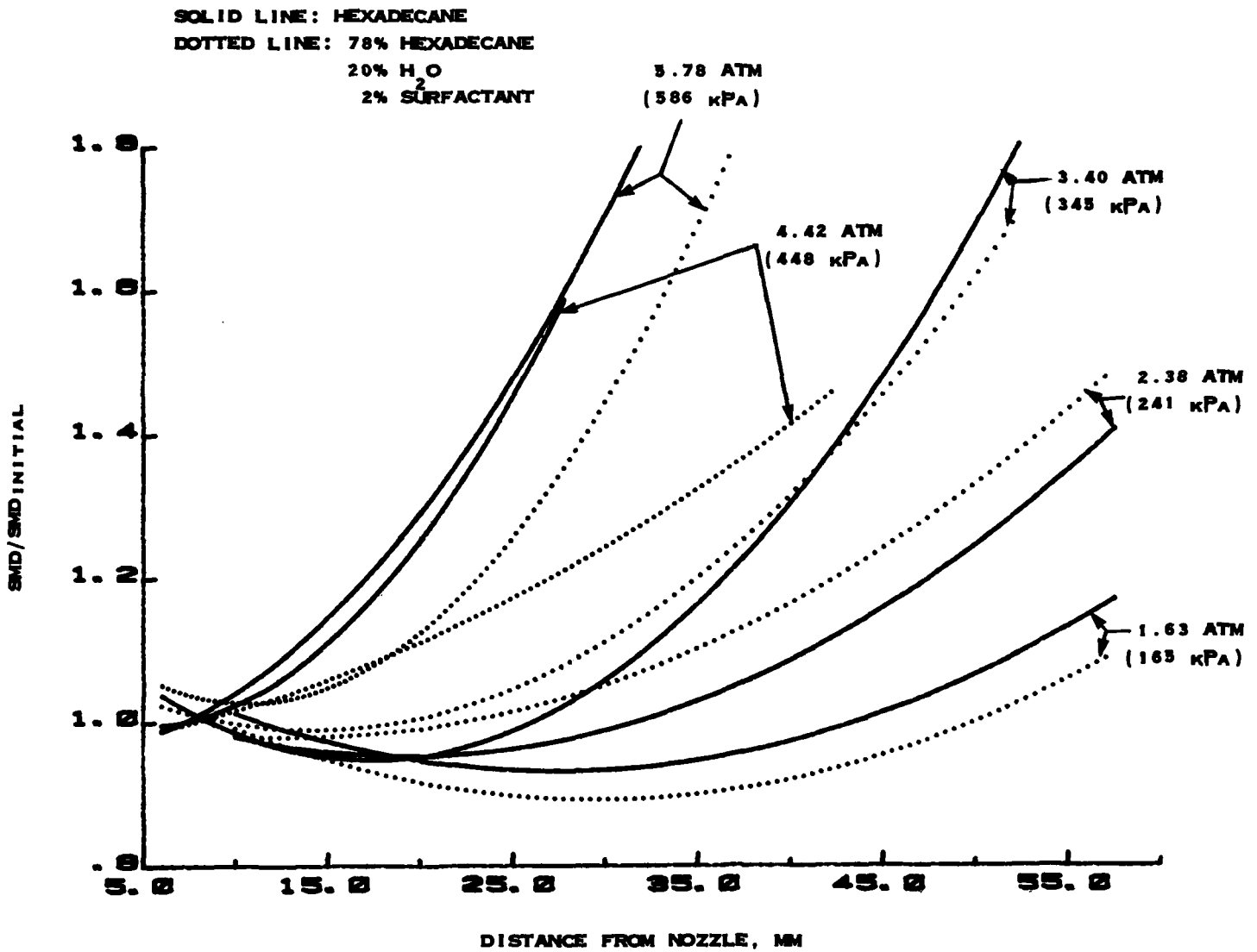


FIGURE 14. RESULTS OF FIGURES 12 AND 13 COMPARED

These trends correspond qualitatively to those expected if the emulsified fuel were undergoing microexplosions when the temperature and/or pressure were raised to a point where the drop temperature exceeded the spontaneous nucleation point of water. Below the spontaneous nucleation point the spray drop sizes should be similar for the two fuels, but as the drop temperature exceeds that condition the emulsified drop may be shattered into many smaller drops producing a smaller SMD than the neat fuel as distances from the nozzle increase.

In order to make this argument quantitative, it is necessary to know the drop temperature as a function of the air temperature and pressure. Presently there are no techniques to measure drop temperatures in a polydisperse spray where the small drops heat up rapidly while the large ones are much slower. This makes it necessary to predict the drop temperatures using the computer model to balance the heat conducted to the drop from the air with the heat used to vaporize the fuel. Some results from the model described earlier are shown in Tables 3 and 4 which indicate the increase in steady-state drop temperature with increasing air temperature or pressure. By comparing those tables with Figures 11 and 14, it may be seen that the drop size distributions for the emulsified and neat fuels diverge at a predicted steady state drop temperature of about 520 K. This may be compared with the limit of superheat of water of about 540 K (Ref. 12). The divergence of drop size distributions for emulsified and neat fuels at a drop temperature somewhat below the limit of superheat is consistent with the microexplosion hypothesis (Ref. 11). As mentioned previously, the limit of superheat is an upper limit where drop fragmentation must occur if water is present, while the probable temperature for spontaneous nucleation of water, and hence, microexplosions to occur is bounded by the normal boiling point (corrected for pressure) on the low end ($\sim$373 K) and the limit of superheat ($\sim$540 K) on the upper end. However, results from the model, which also predicts heat up times, would indicate

only the smaller diameter drops have reached the steady-state temperature at positions where the drop size distributions diverge.

Table 5 represents the computer predicted drop temperatures, (FTEMP) and the other drop information as explained previously for Table 2, for a location (X DROP) 26.4 mm from the nozzle for air conditions of 700 K and 448 kPa (4.42 atm). At these conditions, the results from Figure 11 indicate a considerable divergence between the emulsified and neat fuel SMD's. Although the steady-state temperature is close to the superheat limit of water (540 K) at these conditions, only the drops of initial size smaller than 28.0 μm exceed (approximately) 500 K and they represent about 34 percent of the original liquid volume of the spray. The drops equal to or larger than 177.6 μm represent less than three percent of the liquid volume of the initial spray and can be ignored. Thus, although the steady-state temperature is about 535 K, most of the drops are predicted to reach that temperature only late in their lifetime, and larger drops have only begun to heat up; e.g., the 141μm drop has increased in "uniformly mixed" temperature from 311 K to 324K. Peak surface temperatures in the larger drops are higher, of course, than the uniformly mixed temperature would imply, but the result, nevertheless, is that the larger drops in the spray are, for the conditions of these experiments, much lower in temperature than the steady-state temperature. The variation of drop temperature with size coupled with the uncertainty of the temperature where spontaneous nucleation of the water microdrops should occur (as discussed earlier in the report) makes an exact condition where microexplosions should occur a meaningless exercise. What the model results do reveal is that the steady state drop temperature does increase with increasing air temperature and pressure to a range where spontaneous nucleation probably would occur if the water has not completely evaporated before reaching that condition. The model also indicates a considerable amount of the liquid spray volume which is contained in the larger drops is not at a temperature where microexplosions are expected.

**Table 5. Computer Predicted Spray Characteristics for a Condition of $T_{Air}$ = 700 K, $P_{Air}$ = 448 kPa (4.42 atm), $V_{Air}$ = 8.54 m/s**

| R-R XBAR (UM) | R-R N | CORR.COEF. | SMD |
|---|---|---|---|
| 85.8 | 1.89 | .974 | 45.53 |

| Initial DIAM | DIAM | TIME | X DROP | Y DROP | Z DROP | U-VEL | V-VEL | W-VEL | FTEMP | RE |
|---|---|---|---|---|---|---|---|---|---|---|
| 5.6 | .9 | .00020 | .0069 | .0021 | 0.0000 | 8.540 | .000 | 0.000 | 534.7 | .0 |
| 7.0 | .9 | .00031 | .0080 | .0022 | 0.0000 | 8.540 | -.000 | 0.000 | 534.7 | .0 |
| 8.8 | .9 | .00048 | .0098 | .0024 | 0.0000 | 8.540 | -.000 | 0.000 | 534.7 | .0 |
| 11.1 | .9 | .00073 | .0123 | .0028 | 0.0000 | 8.540 | .000 | 0.000 | 534.7 | .0 |
| 14.0 | .9 | .00111 | .0162 | .0033 | 0.0000 | 8.540 | -.000 | 0.000 | 534.7 | .0 |
| 17.6 | .9 | .00169 | .0219 | .0040 | 0.0000 | 8.540 | .000 | 0.000 | 534.7 | .0 |
| 22.2 | 12.7 | .00205 | .0264 | .0051 | 0.0000 | 8.580 | .030 | 0.000 | 534.7 | .1 |
| 28.0 | 25.9 | .00181 | .0264 | .0066 | 0.0000 | 9.145 | .452 | 0.000 | 498.7 | 2.3 |
| 35.2 | 35.0 | .00158 | .0264 | .0081 | 0.0000 | 10.629 | 1.560 | 0.000 | 444.8 | 10.2 |
| 44.4 | 44.4 | .00142 | .0264 | .0091 | 0.0000 | 12.600 | 3.032 | 0.000 | 400.1 | 26.7 |
| 55.9 | 55.9 | .00134 | .0264 | .0097 | 0.0000 | 14.200 | 4.226 | 0.000 | 370.7 | 49.9 |
| 70.5 | 70.5 | .00130 | .0264 | .0099 | 0.0000 | 15.084 | 4.886 | 0.000 | 351.4 | 75.9 |
| 88.8 | 88.8 | .00128 | .0264 | .0100 | 0.0000 | 15.533 | 5.221 | 0.000 | 338.6 | 105.3 |
| 111.9 | 111.9 | .00126 | .0265 | .0102 | 0.0000 | 15.964 | 5.543 | 0.000 | 329.9 | 143.8 |
| 141.0 | 141.0 | .00124 | .0264 | .0103 | 0.0000 | 16.369 | 5.846 | 0.000 | 324.0 | 193.9 |
| 177.6 | 177.6 | .00122 | .0264 | .0104 | 0.0000 | 16.744 | 6.126 | 0.000 | 319.9 | 258.5 |
| 223.8 | 223.8 | .00121 | .0264 | .0105 | 0.0000 | 17.072 | 6.370 | 0.000 | 317.2 | 340.9 |
| 282.0 | 282.0 | .00120 | .0265 | .0106 | 0.0000 | 17.366 | 6.590 | 0.000 | 315.3 | 446.4 |
| 355.2 | 355.2 | .00119 | .0265 | .0106 | 0.0000 | 17.629 | 6.786 | 0.000 | 314.0 | 581.0 |
| 447.6 | 447.6 | .00118 | .0264 | .0107 | 0.0000 | 17.859 | 6.958 | 0.000 | 313.1 | 752.2 |
| 563.9 | 563.9 | .00117 | .0264 | .0107 | 0.0000 | 18.061 | 7.109 | 0.000 | 312.4 | 969.6 |

The computer model is instructive in predicting and understanding some of the phenomena observed experimentally, but it is not sufficiently complete to compare precisely with the experimental results. The limitations of the current version of the computer code were mentioned earlier in this report and include: (1) no provision for inhomogenities in drop size distribution along the line-of-sight, (2) secondary atomization of drops near the nozzle is ignored, and (3) the weighting factor associated with the laser beam location and size has been omitted. Because of the first two omissions, the model predicts an increase in SMD moving away from the nozzle while the experimental results show an initial decrease except at the highest temperatures. An effort was made to compare the trends for experimental and predicted SMD's by adjusting the initial Rosin-Rammler parameters ($\bar{x}$ and N) so that the predicted $\bar{x}$ and N at 11.4 mm and 16.4 mm were similar to the measured values with the results as shown in Figure 15. Experimentally measured SMD's at 6.4 mm were usually larger than at 11.4 mm while the predicted SMD's were significantly smaller. The fact that the atomization process was not complete at the 6.4 mm location as well as the other omissions from the model just mentioned probably account for that initial discrepancy. It should be noted that the upstream edge of the laser beam is only 2 mm from the nozzle at the 6.4 mm sampling location. There is a considerable discrepancy at the 21.4 mm location for the 700 K case. The discrepancy is probably partly due to an overestimate of the measured SMD due to beam steering problems, and points out the need to measure the amount of fuel vaporized at different locations to further check out the model. A more exact comparison of experimental and model results will require some additional sections to be added to the model to correct the deficiencies cited.

## Drop Size Measurements in Flames

Drop size measurements in burning sprays have been attempted in several configurations including cases where the flame was stabilized in

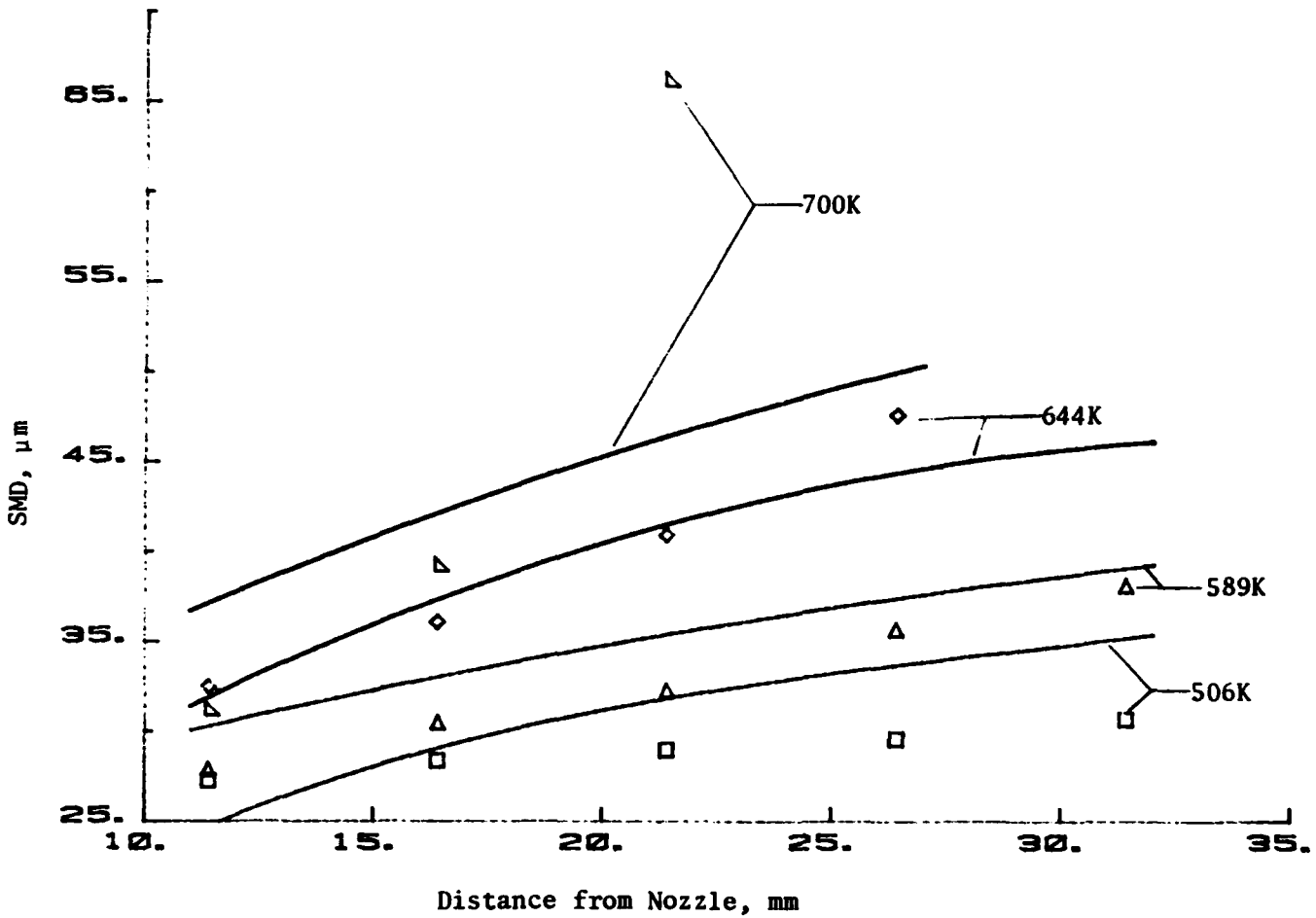


FIGURE 15. COMPARISON OF PREDICTED (LINES) AND MEASURED (SYMBOLS) SMD's AT DIFFERENT AIR TEMPERATURES (P=4.42 atm) (448kPa)

a region downstream from the nozzle. Experiments to date have resulted in inadequate signal-to-noise ratios to determine reasonable drop size distributions. Generally, two types of problems are present when making size measurements with laser-diffraction instrumentation in burning sprays. First, the flame produces high levels of visible and near-infrared radiation (in the response range of the detectors) which is orders of magnitude higher in intensity than the desired scattered radiation from the HeNe laser. Secondly, the severe gradients in temperature and air/fuel vapor concentrations result in serious beam steering problems causing the laser beam to be directed onto areas of the detector other than the central ring. This produces signals which appear to be due to large drops scattering light onto the inner detector rings and thus represents a false signal.

The three modifications described in the EXPERIMENTAL APPARATUS section were sufficient to discriminate against the flame radiation for the cases examined. However, the severe refractive index gradients produced so much noise on the inner detector rings that the drop size data which were computed were judged to be unreasonable. Further consideration is being given to ways to circumvent this problem.

## CONCLUSIONS

Techniques have been developed which allow for the determination of drop-size data in evaporating fuel sprays over a range of elevated pressures and temperatures important to gas-turbine combustion.

It has been determined that there are substantial differences in the evaporation characteristics of emulsified fuels when compared with neat fuels. The spray droplets of the evaporating emulsified fuel are, on the average, significantly smaller than the droplets of neat fuel at corresponding elevated temperature/pressure conditions. The differences are enhanced as the pressure increases for the range examined (to about 5.8 atm (590 kPa)). These findings are consistent with the microexplosion hypothesis but a thorough analysis of other possible effects has not been completed.

Limited experimental data would suggest that the size of drops at initial atomization depends strongly on the air pressure, with SMD $P_{Air}^{-0.4}$.

## RECOMMENDATIONS FOR NEXT YEAR

Results already described have indicated significant differences in drop sizes for evaporating sprays of emulsified and neat fuels. In order to understand the reasons for these differences, the following work is proposed for the next year of this program, although there may be insufficient time to pursue all of these suggestions.

1. Conduct similar atomization/evaporation experiments with single component fuels of lower boiling point than n-hexadecane. Fuels such as n-octane/water emulsions should not exhibit microexplosions but would still be subject to the "heat-sink" effect of water on the evaporation process. This will help to separate the microexplosion effect on drop size from the reduced evaporation rate due to the high heat of vaporization of water.

2. Develop method(s) for measuring fuel vapor concentration in sprays. Both optical and probe techniques have been used by other workers to measure fuel/air ratios in sprays and to differentiate between the liquid and vapor phases of the fuel. These would be useful in studying the evaporation of emulsified fuels, as microexplosions would enhance the evaporation rates while the "heat-sink" effect of water would slow down evaporation rates.

3. Modify computer model for 2-component fuels with various assumptions about relative evaporation rates. The effect of water emulsification with a single component fuel could be studied from a theoretical view to compare with the experimental results.

4. Modify computer model to include the inhomogeniety of spray, and laser beam location and intensity profile. This would lead to a better capability to compare experimental and computer predicted results.

5. Modify computer model to predict the concentration of fuel vapor as a function of axial distance from the nozzle. If the measurement techniques described in item (2.) are developed, they could be compared with the predicted results.

## ACKNOWLEDGMENTS

This work has resulted from contributions of a large number of people, whose efforts we wish to acknowledge. The Office of Naval Research, with technical monitoring by M.K. Ellingsworth, provided funds for this program under Contract No. N0014-80-K-0460. Mr. R.C. Haufler performed much of the experimental work. Much of the computer model was based on work done by Professors J.S. Chin and A.H. Lefebvre at Purdue and W.H. Ayers, J. Swithenbank, and F. Boyson of the University of Sheffield. Assistance in the computer programming was provided by Mr. T.J. Callahan. Dr. B. Weiner of Malvern provided ideas in the use of the drop sizing instrument. Electronics necessary for this program were designed by S.A. Cerwin and constructed by H.F. Donoho, Jr. Dr. D.W. Naegeli at this laboratory and Dr. J.J. Sangiovanni of UTRC provided helpful ideas and Ms. S.J. Boyd and Mr. J.W. Pryor helped in manuscript preparation.

## REFERENCES


1. Moses, C.A., "Reduction of Exhaust Smoke from Gas Turbine Engines by Using Fuel Emulsions-II," presented at the Western States Section of the Combustion Institute, University of California, La Jolla, California, 18 October 1976.

2. Klarman, A.F., Rollo, A.J., and Scott, H.C., "Evaluation of Water/Fuel Emulsion Concept for Test Cell Smoke Abatement," Naval Air Propulsion Center, Trenton, New Jersey, Report No. NAPC-PE-7, March 1978.

3. Dodge, L.G., and Moses, C.A., "Mechanisms of Smoke Reduction in the High Pressure Combustion of Emulsified Fuels: Vol I: Construction of Apparatus and Preliminary Experiments," Interim Report No. MED130, Contract No. N00014-80-K-0460, October 1981.

4. Chin, J.S., and Lefebvre, A.H., "The Role of the Heat-Up Period in Fuel Drop Evaporation," to be published.

5. Spalding, D.B., "The Combustion of Liquid Fuels," Fourth Symposium (International) on Combustion, Williams and Wilkins Co., pp. 847-864, 1953.

6. Frossling, N., "On the Evaporation of Falling Droplets", Gerlands Beitrage zur Geophysik, Vol. 52, pp. 170-216, 1938.

7. Law, C.K., "A Model for the Combustion of Oil/Water Emulsion Droplets," Combustion Science and Technology, Vol. 17, 1977, pp. 29-38.

8. Birchley, J.C., and Riley, N., "Transient Evaporation and Combustion of a Composite Water-Oil Droplet," Combustion and Flame, Vol. 29, 1977, p. 145.

9. Jacques, M.T., "Transient Heating of an Emulsified Water-in-Oil Droplet," Combustion and Flame, Vol. 29, 1977, p. 77.

10. Gollahalli, S.R., "An Experimental Study of the Combustion of Unsupported Drops of Residual Oils and Emulsions," Combustion Science and Technology, Vol. 19, 1979, pp. 245-250.

11. Avedisian, C.T., "Spontaneous Nucleation in Droplet Combustion," ASME Paper No. 81-WA/HT-43, 1981.

12. Blander, M., and Katz, J.L., "Bubble Nucleation in Liquids," AIChE Journal, Vol. 21 No. 5, 1975, pp. 833 848.

13. Chin, J.S., and Lefebvre, A.H., "Steady State Evaporation Characteristics of Hydrocarbon Fuel Drops," AIAA-82-1176, presented at the AIAA/SAE/ASME 18th Joint Propulsion Conference, June 21-23, 1982.

14. Anon., Technical Data Book - Petroleum Refining, Second Edition, American Petroleum Institute, Division of Refining, Washington, D.C., 1970.

15. Boyson, F., and Swithenbank, J., "Spray Evaporation in Recirculating Flow," Seventeenth Symposium (International) on Combustion, The Combustion Institute, 1979, pp. 443-453.

16. Dickerson, R.A., and Schuman, M.D., "Rate of Aerodynamic Atomization of Droplets, J. Spacecraft and Rockets," January - February 1965, pp. 99-100.

17. Allen, T., Particle Size Measurement, Third Edition, Chapman and Hall, 1981, pp. 139, 140.

## APPENDIX A

## FUEL SPRAY COMPUTER MODEL - MATHEMATICS

For purposes of discussion, the model is divided into three parts called (1) Thermodynamics, (2) Aerodynamics, and (3) Drop-Size Distribution. Each section is discussed in order. An overall flow chart is shown in Figure A-1.

### Thermodynamics

This part of the model computes the heat-up of the drop, the final steady-state temperature, and the fuel and air properties necessary for those calculations. This part of the model is identical to that described by Chin and Lefebvre (Ref. A1 and A2) except that some of the fuel property data were taken from the American Petroleum Institute Data Book (Ref. A3). The results from this model are very similar to those presented by Chin and Lefebvre when the model is used for quiescent fuel sprays. The integration of this part of the model with the other sections to be described allows the examination of sprays in situations where both spray and air are moving with a nonzero relative velocity. The mathematics are outlined below, but a more detailed derivation is given by Chin and Lefebvre (Ref. A1 and A2) which in turn is based on the theories described by Spalding (Ref. A4).

The steady-state temperature is determined as follows. The mass transfer rate, $\dot{m}$, from a drop is given by,

$$\dot{m}_F = 2\pi D \, (k_g/c_{p,g}) \quad \ln (1+B) \tag{A1}$$

where D is the diameter, $k_g$ is the thermal conductivity of the gas, $c_{p,g}$ is the specific heat at constant pressure, and B is either $B_M$, the mass diffusion transfer number if mass diffusion is controlling, or $B_T$, the

FIGURE A-1 FLOW CHART OF SPRAY MODEL

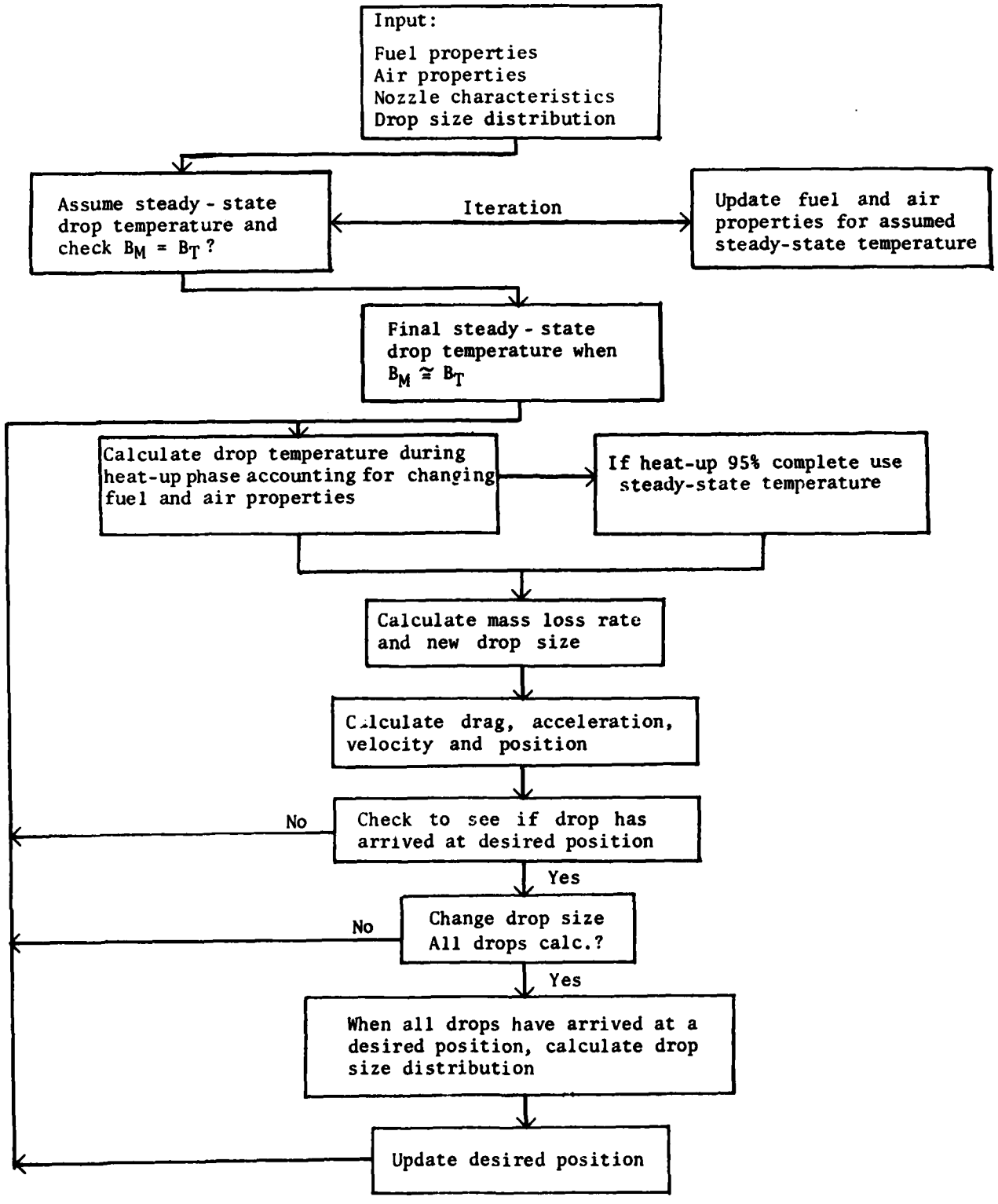

thermal diffusion transfer number if heat transfer is controlling and the Lewis number is assumed to be unity. $B_M$ is defined as

$$B_M = (Y_{F,s} - Y_{F,\infty}) / (1 - Y_{F,s}) \quad \text{(A2)}$$

where $Y_{F,s}$ and $Y_{F,}$ are the fuel mass fractions at the drop surface and in the ambient air, respectively, and $Y_{F,s}$ is

$$Y_{F,s} = P_{F,s} M_F / (P_{F,s} M_F + (P - P_{F,s}) M_A) \quad \text{(A3)}$$

where $P_{F,s}$ is the fuel vapor pressure at the drop surface, P is the ambient pressure, and $M_F$ and $M_A$ are the molecular weights of fuel and air, respectively. The vapor pressure was calculated using the method recommended by the American Petroleum Institute Data Book (Ref. A3) called Procedure 5A1.10, "Vapor Pressures of Pure Hydrocarbons."

The thermal diffusion transfer number $B_T$ for an evaporating drop is

$$B_T = c_{p,g} (T_\infty - T_s) / L \quad \text{(A4)}$$

where $T_\infty$ and $T_s$ are the ambient air temperature and drop surface temperature and L is the latent heat of fuel vaporization corrected from the normal boiling point to the actual surface temperature.

The accuracy of Equation (A1) is very dependent on the choice of values for $k_g$ and $c_{p_g}$. As recommended by Chin and Lefebvre (Ref. A1) a reference temperature was chosen as the drop surface temperature plus 1/3 of the difference between ambient air and surface temperatures. Similarly a reference value of the fuel vapor mass fraction was taken as the value just outside the surface plus 1/3 of the difference between the value at infinity and just outside the surface. Using these reference conditions denoted by "r" the specific heat of the gas is given by,

$$c_{p,g} = Y_{A,r} \, (c_{p,A} \text{ at } T_r) + Y_{F,r} \, (c_{p,V} \text{ at } T_r) \tag{A5}$$

and the thermal conductivity by,

$$k_g = Y_{A,r} \, (k_A \text{ at } T_r) + Y_{F,r} \, (k_V \text{ at } T_r) \tag{A6}$$

At steady-state conditions, $B_M = B_T$ or from Equations (A2) and (A4)

$$\frac{Y_{F,s} - Y_{F,\infty}}{1 - Y_{F,s}} = \frac{c_{p,g} \, (T_\infty - T_{s,st})}{L} \tag{A7}$$

where $T_{s,st}$ is the desired surface temperature under steady-state conditions. Assuming that the fuel vapor concentration in the ambient air is zero ($Y_{F,\infty} = 0$) and substituting for $Y_{F,s}$ from Equation (A3) then (A7) becomes

$$\frac{P}{P_{F,s}} - \frac{M_F}{M_A} \frac{L}{c_{p,g} \, (T_\infty - T_{s,st})} - 1 = 0 \tag{A8}$$

In solving Equation (A8) to determine the steady-state surface temperature $T_{s,st}$, some of the variables can be specified, P, $M_F$, $M_A$, and $T_\infty$ but the remaining three variables are functions of temperature, with L being related to the heat of vaporization at the normal boiling point $L_{T,bn}$ by,

$$L = L_{T,bn} \left[ (T_{cr} - T_s) \, / \, (T_{cr} - T_{bn}) \right]^{0.38} \tag{A9}$$

where $T_{cr}$ is the critical temperature and $T_{bn}$ is the normal boiling point of the fuel. In order to solve (A8) it is necessary to first assume a value for $T_{s,st}$. That temperature is used to calculate a reference temperature $T_r$ which in turn is used to calculate those quantities specified in Equations (A5) and (A6) used to calculate $c_{p,g}$ and $k_g$, and to calculate L as specified in (A9). If the assumed value of $T_{s,st}$ is too low, the left side of Equation (A8) will be positive. An iterative procedure must be used to continue specifying $T_{s,st}$ until Equation (A8) is satisfied within the desired accuracy. That procedure results in a

determination of the steady state surface temperature $T_{s,st}$ and the transfer number $B=B_M=B_T$. The steady state quiescent evaporation constant $\lambda_{q,st}$ can then be determined from,

$$\lambda_{q,st} = 8\ k_g\ \ln\ (1+B)\ /\ \rho_F\ c_{p,g} \qquad \text{(A10)}$$

where $\rho_F$ is the fuel density. Frossling (Ref. A5) has shown that convective effects can be accounted for in the case where heat transfer rates are controlling by,

$$\lambda_{c,st} = \lambda_{q,st}\ (1 + 0.276\ Re_D^{0.5}\ Pr_g^{0.33}) \qquad \text{(A11)}$$

where $\lambda_{c,st}$ is the steady-state evaporation constant corrected for convective effects, $Pr_g$ is the Prandtl number for the gas, and $Re_D$ is the Reynolds number using the relative velocity between the drop and the gas. This velocity should include a fluctuating component in the case of turbulent flow. Turbulence intensities were not measured in these experiments, but a value of 20 percent of the axial velocity was used as an estimate. The effective velocity used to calculate $Re_D$ for the evaporation calculation was taken as the sum of the fluctuating component (20 percent of the air velocity) plus the difference between the drop and air velocities. These computations specify the steady-state properties of the drop.

The evaporation which occurs during the drop heat-up period is significant in many practical situations, with the drop being completely evaporated before reaching steady-state conditions is some instances. Chin and Lefebvre (Ref. A2) have predicted that high air pressures and convective effects, which are often absent in laboratory experiments, both tend to increase the relative importance of the heat-up period relative to the steady-state phase of drop evaporation. Because the experiments conducted in this study were of real sprays at high pressures and relative velocities, it was necessary to model the heat-up period in detail.

Chin and Lefebvre (Ref. A2) have shown that the rate of change of drop surface temperature is given by,

$$dT_S / dt = (\dot{m}_F L / c_{p,F} m) \{ (B_T / B_M) - 1 \) \quad (A12)$$

where $\dot{m}_F$ is specified by Equation (A1) with $B=B_M$ during the heat-up period, and $\dot{m}$ is the drop mass,

$$m = (\pi/6) \rho_F D^3 \quad (A13)$$

The change of drop size with time is given by (Ref. A2),

$$dD / dt = -4 k_g \ln (1+B_M) / \rho_F c_{p,g} D \quad (A14)$$

The drop temperature asymptotically approaches the steady-state temperature, and it was assumed that when the temperature had risen to 95 percent of the difference between the initial fuel temperature and the steady-state temperature, that the heat-up calculations could be terminated and steady-state properties used.

## Aerodynamics

The approach used was a much more simplified version of the one developed at the University of Sheffield and described in several papers, e.g., Boyson and Swithenbank (Ref. A6). A cylindrical coordinate system was used where x is the axial distance, y the radial distance, and z the angular position, with corresponding velocities in the axial (u), radial (v), and tangential (w) directions. For this work, the tangential velocities were assumed zero.

The equations of motion of a particle (drop) neglecting all forces except drag, are,

$$\dot{u}_p = -F (u_p - u_\infty) \quad (A15)$$

$$\dot{v}_p = \frac{w_p^2}{y_p} - F\,(v_p - v_\infty) \tag{A16}$$

$$\dot{w}_p = \frac{v_p\, w_p}{y_p} - F\,(w_p - w_\infty) \tag{A17}$$

where the "p" subscripts refer to the particle and the "∞" subscript refers to the free stream, and F is given by,

$$F = (18\,\mu g\,/\,\rho_p\, D_p^2)\;(C_D\, Re\,/\,24) \tag{A18}$$

where $\mu_g$ is the gas viscosity, $\rho_p$ is the particle density, $D_p$ is the particle diameter, $C_D$ is the drag coefficient, and Re is the Reynolds number defined as,

$$Re = \frac{D_p\, \rho_g}{\mu_g} \left| \vec{u}_p - \vec{u}_\infty \right| \tag{A19}$$

The drag coefficient, $C_D$, is given by (Ref. A7),

$$C_D = 27\, Re^{-0.84} \qquad 0 \;\; Re \leq 80 \tag{A20}$$

$$C_D = 0.271\, Re^{0.217} \qquad 80 < Re \leq 10^4 \tag{A21}$$

$$C_D = 2 \qquad 10^4 > Re \tag{A22}$$

The equations of motion (A15 to A17) are solved numerically using a step size of 1 to 10 μs, and the equations of trajectory are solved in a similar manner,

$$\dot{x}_p = u_p \tag{A23}$$

$$\dot{y}_p = v_p \tag{A24}$$

$$\dot{z}_p = \frac{w_p}{y_p} \tag{A25}$$

These equations describe the trajectory of a particle in a gas stream. For each iteration in the trajectory calculation, the drop size and temperature are updated using the procedure described in the Thermodynamics section.

At the end of each iteration through the trajectory calculations, the current calculated axial position of the particle is checked against a target value. When the particle reaches that target value for axial position, the position, transit time, size, temperature, and other parameters for that drop are frozen and the calculations are repeated for the next larger drop size. After all drops reach a targeted axial position, corresponding to a measurement location, the drop size distribution is calculated, important data are printed out, the target position is moved downstream, and the calculations are repeated.

**Drop Size Distribution**

The computer model makes all calculations on individual drops of certain sizes, but the instrumentation used to measure the spray works best in characterizing the drop sizes by two parameters which specify a size and width of the distribution. Three distributions may be selected: normal, log-normal, and Rosin-Rammler. The Rosin-Rammler distribution has provided the best fit of the sprays studied and has been used throughout this program. In order to compare the predictions from the computer model with the experimental results, it is necessary to convert the computer predicted drop sizes at a given location into an equivalent set of two parameters specifying the Rosin-Rammler distribution.

If R represents the fraction of the liquid being sprayed contained in drops larger than diameter D, then for the Rosin-Rammler distribution (Ref. A8),

$$R = \exp\left(-(D / \bar{x})^N\right) \tag{A26}$$

where $\bar{x}$ represents a size, and N specifies the width of the distribution. It is convenient to specify a spray by a single parameter representing an "average" drop size. However, a straight numerical average is heavily weighted towards the smallest drops which are extremely plentiful but which contain a very small fraction of the total volume of the liquid. For combustion processes, the surface-to-volume ratio is important to evaporation, so an average drop size may be chosen which has a surface-to-volume ratio representative of the actual spray, and such an average is called the surface-volume mean diameter or Sauter mean diameter (SMD). The SMD is related to the Rosin-Rammler parameters by (Ref. A8),

$$SMD = \bar{x} / \Gamma(1-1/N) \qquad N>1 \tag{A27}$$

Specifying $\bar{x}$ and N allows the calculation of the SMD, or specifying SMD and N determines $\bar{x}$.

An initial set of drop sizes distributed approximately exponentially in size (i.e., evenly spaced when plotted as ln D) and covering the range of about 6μm to 560μm (corresponding to the response range of the drop sizing instrument) with 16 to 21 different sizes is used in the model. Assuming size classes bounded by these drops as end points, the initial fraction of liquid contained in drops larger than a certain size class is given by Equation (A26).

$$R_i = \exp\left(-(D_{o,i} / \bar{x})^N\right) \qquad 1 \le i \le n \tag{A28}$$

$$R_o \equiv 1$$

$$R_{n+1} \equiv 0$$

where "n" is the number of drops, $D_o$ is the initial drop diameter, and the initial fraction of liquid in each size class is,

$$F_{o,i} = R_i - R_{i+1} \qquad o \leq i \leq n \qquad \text{(A29)}$$

$$F_{o,-1} \equiv 0$$

After evaporation begins, the small drops begin evaporating quickly while the large ones evaporate slowly, changing the fraction of liquid in the different size classes unevenly. Denoting the smallest nonevaporated drop size by "k", the fraction of liquid remaining in any size class is,

$$F_i = \frac{F_{o,i} \left\{ (D_i / D_{o,i})^3 / u_{p,i} + (D_{i+1} / D_{o,i+1})^3 / u_{p,i+1} \right\} /2}{\sum_{j=k}^{n} F_{o,j} \left\{ (D_j / D_{o,j})^3 / u_{p,i} + (D_{j+1} / D_{o,j+1})^3 / u_{p,j+1} \right\} /2} \qquad \text{(A30)}$$

where $k \leq i \leq n$ $(o \leq k \leq n)$

$$D_0 \equiv D_1$$

$$u_{p,0} \equiv u_{p,1}$$

$$D_{n+1} \equiv D_n$$

$$u_{p,n+1} \equiv u_{p,n}$$

and $u_{p,i}$ is the axial velocity of the ith drop, $D_i$ is the instantaneous drop size, and $D_{o,i}$ is the initial drop size of the ith drop. Each size class is characterized by the drops making up the end points, and the initial fraction of liquid in a size class is modified by the average loss of volume of the end point drops. The velocity term is added to account for the fact that as the drops slow down they increase their relative concentration, and thus their weighting factor, in the sample volume.

The cumulative fraction of liquid in all size classes including and larger than the ith class is,

$$R_i = \sum_{j=i}^{n} F_i \qquad k \le i \le n \qquad \text{(A31)}$$

This instantaneous value of $R_i$ is related to the drop sizes and Rosin-Rammler parameters by Equation (A28) with the initial drop size $D_{o,i}$ replaced by the instantaneous value $D_i$,

$$R_i = \exp\left(-(D_i / \bar{x})^N\right) \qquad k \le i \le n \qquad \text{(A32)}$$

Taking the natural logarithm of both sides twice and excluding i=k ($R_i$=1), Equation (A32) becomes,

$$\ln_e(\ln_e(1 / R_i)) = N \ln_e D_i - N \ln_e \bar{x} \qquad k+1 \le i \le n \qquad \text{(A33)}$$

This has the form of the equation of a straight line, y=mx+b, if the following definitions are used,

$$y = \ln_e(\ln_e(1/R))$$

$$m = N$$

$$x = \ln_e D$$

$$b = -N \ln_e \bar{x}$$

Thus, by determining a least squares fit of the straight line through the data $\ln_e(\ln_e(1/R_i))$ versus $\ln_e D_i$, the Rosin-Rammler parameters are given by,

$$N = m \text{ (the slope)} \qquad \text{(A35)}$$

and

$$\bar{x} = \exp(-b / N)$$

A standard routine is used to perform the least squares operation and the Rosin-Rammler parameters and the SMD (from Equation (A27)) are determined at each target value of the axial location corresponding to the position where experimental data are obtained. Although the initial distribution at the nozzle is an ideal Rosin-Rammler distribution, the distribution downstream does not correspond exactly to the Rosin-Rammler equation due to the different evaporation rates for the different sized drops, and the degree of fit is determined by the correlation coefficient of the straight line through the computed data.

## APPENDIX A
## REFERENCES


A1. Chin, J.S., and Lefebvre, A.H., "Steady State Evaporation Characteristics of Hydrocarbon Fuel Drops," AIAA-82-1176, presented at the AIAA/SAE/ASME 18th Joint Propulsion Conference, June 21-23, 1982.

A2. Chin, J.S., and Lefebvre, A.H., "The Role of the Heat-Up Period in Fuel Drop Evaporation," to be published.

A3. Anon., Technical Data Book - Petroleum Refining, Second Edition, American Petroleum Institute, Division of Refining, Washington, D.C., 1970.

A4. Spalding, D.B., Some Fundamentals of Combustion, Butterworths Scientific Publications, 1955.

A5. Frossling, N., "On the Evaporation of Falling Droplets", Gerlands Beitrage zur Geophysik, Vol. 52, pp. 170-216, 1938.

A6. Boyson, F., and Swithenbank, J., "Spray Evaporation in Recirculating Flow," Seventeenth Symposium (International) on Combustion, The Combustion Institute, 1979, pp. 443-453.

A7. Dickerson, R.A., and Schuman, M.D., "Rate of Aerodynamic Atomization of Droplets," J. Spacecraft and Rockets," January - February 1965, pp. 99-100.

A8. Allen, T., Particle Size Measurement, Third Edition, Chapman and Hall, 1981, pp. 139, 140.

# APPENDIX B

## FUEL SPRAY COMPUTER MODEL - LISTING

```
&DROPP T=00004 IS ON CR TR   USING 00068 BLKS R=0000

0001  FTN4,L,Q
0002        PROGRAM DROPP
0003  C THIS DROP EVAPORATION MODEL INCORPORATES MUCH OF THE HEAT TRANSFER
0004  C SUGGESTED BY CHIN AND LEFEBVRE IN AIAA-82-1176  -  8/30/82
0005        DIMENSION D(23),DIAM0(23),TIME(23),XP(23),YP(23),ZP(23),UP(23),
0006       C VP(23),WP(23),FF0(24),FF(24),R(24),FTEMP(23),RE(23),NU(23),
0007       C F(24),CB(23),CD(23),XDATA(23),YDATA(23),ZDATA(23),DMU(23),
0008       C XK(23),REN(25),
0009       & TSD(23),LAMBHU(23),LAMBA(23)
0010        REAL L,LAMBST,NU,MUA,N,NNEW,M,LTBN,MWA,MWF,LEFT,KA,KV,KG,MUG,MUV,
0011       & LAMBHU,LAMBA,MASSD,MDOT
0012  C DROP DIAMETERS (M)
0013        DATA DIAM0/5.8,7.2,9.0,11.4,14.4,18.4,23.6,30.3,38.9,50.1,
0014       C 64.6,84.2,112.8,160.3,261.6,563.9/
0015        NDROP = 16
0016        DO 10 I=1,NDROP
0017    10  DIAM0(I) = DIAM0(I) / 1E6
0018  C ALTERNATE SET OF DROP DIAMETERS
0019        NDROP = 21
0020        DO 12 I = 1,NDROP
0021        QQ = (I-1)/3.0
0022    12  DIAM0(I) = 5.5505428 * (2.0**QQ) * 1.0E-6
0023  C STEP SIZE FOR TARGET VALUE AND FINAL TARGET VALUE  (M)
0024        DATA XPT/.00500/
0025        DATA XPTT/.05635/
0026        DATA XPS/.00135/
0027        DATA II/0/
0028        DATA KK/0/
0029  C MASS FRACTION OF FUEL IN AMBIENT AIR SURROUNDING DROP
0030        DATA YFI/0.0/
0031  C FUEL INLET TEMPERATURE (K)
0032        DATA FTEMP0/311./
0033  C BOILING POINT OF FUEL (K)
0034        DATA TBN /560.0/
0035  C EXPANSION COEFF OF FUEL
0036        DATA CEX/0.00055/
0037  C CONE ANGLE OF SPRAY (DEGREES)
0038        DATA PHI/45./
0039  C DISTANCE FROM NOZZLE TO SHEET BREAKUP  (M)
0040        DATA DBREAK/0.005/
0041  C SWIRL COMPONENT OF SPRAY (DEGREES)
0042        DATA FSWIRL/0.0/
0043  C INITIAL SPRAY VELOCITY  (M/S)
0044        DATA VSPRAY/20.76/
0045  C MOLECULAR WEIGHT OF AIR
0046        DATA MWA/28.96/
0047  C INLET AIR VELOCITY, X,Y,Z COMP  (M/SEC)
0048        DATA UA,VA,WA/08.54,0.,0./
0049  C STEP SIZE FOR TIME (SEC)
0050        DATA DELTAT/0.000010/
0051  C LATENT HEAT OF VAPORIZATION AT NORMAL BOILING POINT (KJ/KG)
0052        DATA LTBN/224./
0053  C FUEL DENSITY (KG/M**3)
0054        DATA RHOF0/776.6/
0055  C  MOLECULAR WEIGHT OF FUEL
0056        DATA MWF/226.43/
0057  C  NUMBER OF CARBON ATOMS IN FUEL MOLECULE
0058        DATA NOCARB/16/
```

```
0059  C SURFACE TENSION OF FUEL (NT/M)
0060        DATA SIGMA/28.0E-3/
0061  C CRITICAL TEMP OF FUEL (K)
0062        DATA TCR/720.6/
0063  C  CRITICAL PRESSURE OF FUEL (KPA)
0064        DATA PCR/1421./
0065  C  CRITICAL DENSITY OF FUEL (KG/M**3)
0066        DATA RHOCR/239.0/
0067  C  CRITICAL COMPRESSIBILITY OF FUEL
0068        DATA ZCR/0.225/
0069  C  ACENTRIC FACTOR FOR FUEL (USED TO CALCULATE VAPOR PRESSURE)
0070  C  SEE API DATA BOOK, CHAPTER 2
0071        DATA ACENTR/0.7418/
0072        WRITE (1,999)
0073   999  FORMAT ("ATEMP0(K) =, AIR PRESS(ATM) = ")
0074        READ (1,*) ATEMP0,P
0075        WRITE (1,990)
0076   990  FORMAT (" XBAR (MICRONS)=,  N =, ")
0077        READ (1,*) XBAR,N
0078        XBAR = XBAR * 1.0E-6
0079        WRITE (6,996) ATEMP0,P
0080   996  FORMAT ("ATEMP0(K) =",F6.0,"   AIR PRESS(ATM) = ",F6.2)
0081  C  CONVERT PRESSURE TO KPA
0082        P = P * 101.325
0083        TAI= ATEMP0
0084  C CALCULATE QUANTITIES WHICH ARE INDEP OF DROP SIZE
0085        DO 14 I = 1,NDROP
0086     14 TIME(I) = 0.0
0087  C SET INITIAL DROP ARRAY VALUES
0088        XP0 = DBREAK * COS(PHI * 3.1415/360.)
0089        YP0 = DBREAK * SIN(PHI * 3.1415/360.)
0090        ZP0 = 0.
0091  C SPRAY VELOCITY COMPONENTS
0092        UP0 = VSPRAY * COS(PHI * 3.1415/360.) * COS(FSWIRL*2*3.1415/360.)
0093        VP0 = VSPRAY * SIN(PHI * 3.1415/360.) * COS(FSWIRL*2*3.1415/360.)
0094        WP0 = VSPRAY * SIN(FSWIRL * 2*3.1415/360.)
0095        DO 15 I = 1,NDROP
0096        D(I) = DIAM0(I)
0097        FTEMP(I) = FTEMP0
0098        UP(I) = UP0
0099        VP(I) = VP0
0100        WP(I) = WP0
0101        XP(I) = XP0
0102        YP(I) = YP0
0103        ZP(I) = ZP0
0104     15 R(I) = EXP(-((DIAM0(I)/XBAR)**N))
0105        R(0) = 1.0
0106        R(NDROP+1) = 0.0
0107        DO 90 I = 0,NDROP
0108        FF0(I) = R(I) - R(I+1)
0109     90 CONTINUE
0110        FF0(-1) = 0.0
0111  C  OUTPUT INITIAL VALUES
0112        XBARMU = XBAR * 1E4
0113        WRITE (6,95) XBARMU,N,FTEMP0,TBN,PHI,VSPRAY,UP0,VP0,WP0
0114     95 FORMAT (F6.1,F5.2,2F6.0,F6.1,F7.0,3F7.1)
0115        WRITE (6,96) ATEMP0,UA,VA,WA
0116     96 FORMAT (4F12.1)
0117        WRITE (6,97) DELTAT,P,XP0,YP0,ZP0
0118     97 FORMAT (F8.5,F5.1,3F8.2)
```

```
0119  C  COMPUTE TSST, THE STEADY STATE DROPLET TEMPERATURE (K); ALSO LAMBST
0120  C  THE STEADY STATE EVAPORATION CONSTANT (M**2/S)
0121     99 CONTINUE
0122        TSL = 200.
0123        TSH =TCR-1.
0124        IF (TSH.GT.TAI) TSH=TAI-1.
0125        DO 1000 I=1,100
0126        IF (I.EQ.1) GO TO 1010
0127        IF (I.EQ.2) GO TO 1020
0128        TS = (TSL + TSH) / 2.
0129        GO TO 1030
0130   1010 TS = TSL
0131        GO TO 1030
0132   1020 TS = TSH
0133   1030 CONTINUE
0134        TR = TS + (1./3.) * (TAI - TS)
0135        L = LTBN * ((TCR-TS)/(TCR-TBN))**0.38
0136  C  THIS EXPRESSION TO BE USED ONLY WHEN DATA FOR FOLLOWING EXPRESSION
0137  C  NOT AVAILABLE
0138        PFS =101.325*EXP(2.30259*(-16.188+32.124*TS/TBN-20.704*(TS/TBN)**2
0139       C  +4.768*(TS/TBN)**3))
0140        TREDUC = TS/TCR
0141        A = 36/TREDUC - 35. - TREDUC**6 + 96.73*ALOG10(TREDUC)
0142        B = ALOG10(TREDUC) - 0.0364*A
0143        C = 7*ALOG10(TREDUC) - 0.118*A
0144        TERM1 = C - 1.192*B
0145        TERM2 = 4.93*B
0146        PREDUC = EXP(2.30259 * (TERM1 + ACENTR * TERM2))
0147        PFS = PREDUC * PCR
0148        PDIFF = P - PFS
0149        IF (PDIFF.LT.0.0) PDIFF = 0.0
0150        YFS = PFS*MWF / (PFS*MWF + PDIFF*MWA)
0151        YFR = YFS + (1./3.)*(YFI-YFS)
0152        YAR = 1. - YFR
0153        IF (TR.GT.600.) GO TO 1040
0154        CPA = 4.184 * (0.244388 - 4.20419E-5 * TR + 9.61128E-8 * TR**2
0155       & - 1.16383E-11 * TR**3)
0156        GO TO 1050
0157   1040 CPA = 4.184 * (0.208831 + 7.71027E-5 * TR - 8.56726E-9 * TR**2 -
0158       & 4.75772E-12 * TR**3)
0159   1050 CONTINUE
0160        CPV = (0.363 + 0.000467*TR) * (5. - 0.001*RHOF0)
0161        CPG = YAR * CPA + YFR * CPV
0162        LEFT = (P/PFS) - (MWF/MWA)*L/(CPG*(TAI-TS)) -1.
0163        IF (I.LT.3) GO TO 1060
0164        IF (ABS(LEFT).LT.0.005) GO TO 1083
0165        IF (LEFT.LT.0.0) GO TO 1080
0166        TSL = TS
0167        GO TO 1000
0168   1080 TSH = TS
0169   1060 IF (I.EQ.1.AND.LEFT.LT.0.0) GO TO 1099
0170        IF (I.EQ.2.AND.LEFT.GT.0.0) GO TO 1099
0171   1000 CONTINUE
0172   1083 WRITE(6,1081)
0173   1081 FORMAT(" TS, TSL, TSH, LEFT, P, PFS, L, CPG ")
0174        WRITE(6,*) TS,TSL,TSH,LEFT,P,PFS,L,CPG
0175   1070 TSST = TS
0176        WRITE(1,1075) TSST,LEFT
0177   1075 FORMAT(F10.2,F15.3)
0178        IF (TR.GT.850.) GO TO 1100
```

```
0179          KA = 1.E-4 * (1.13841E-3 + 1.01789E-3*TR - 5.82577E-7*TR**2 +
0180         & 2.46855E-10*TR**3)
0181          GO TO 1110
0182    1100 KA = 1.E-4 * (-.0999992 + 1.19034E-3*TR - 5.29096E-7*TR**2 +
0183         & 1.11208E-10*TR**3)
0184    1110 CONTINUE
0185          E = 2.- 0.0372*(TR/TBN)**2
0186          KV = 1.E-6 * (13.2 - 0.0313 *(TBN-273.)) * (TR/273.)**E
0187          KG = YAR * KA + YFR * KV
0188          WRITE(1,1111)
0189    1111 FORMAT(" KG,KA,KV,YAR,YFR,E,TR ")
0190          WRITE(1,*) KG,KA,KV,YAR,YFR,E,TR
0191          BM = (YFS - YFI) / (1 - YFS)
0192          BT = CPG * (TAI - TSST) / L
0193          RHOFT = RHOF0 * (1 - 1.8*CEX*(TS-288.6) - (0.090*(TS-288.6)**2
0194         & / (TCR - 288.6)**2))
0195          LAMBST = 8 * ALOG(1+BM) / (RHOFT * (CPG/KG))
0196    C DENSITY OF AIR (KG/M**3)
0197          ZAIR = 1.0
0198    101   H = (0.003103/TR) * P / ZAIR
0199          ZAIRN = (1./(1.-H)) - (7349./TR**1.5) * (H/(1.+H))
0200          IF (ABS((ZAIRN-ZAIR)/ZAIRN).LT.0.0005) GOTO 102
0201          ZAIR = ZAIRN
0202          GOTO 101
0203    102   CONTINUE
0204          RHOA = MWA / ZAIR * (P/(8.314*TR))
0205    C   DENSITY OF FUEL VAPOR (KG/M**3)
0206          CALL VPRDN (TCR,PCR,MWF,TR,P,RHOV)
0207    C VISCOSITY OF AIR (KG/M*S) SUTHERLAND CORRELATION
0208          MUA = 1.425E-6 * SQRT(TR) /(1 + (100/TR))
0209    C   VISCOSITY OF THE FUEL VAPOR AND MIXTURE WITH AIR (KG/M*S)
0210          CALL VPRVS(TR,TCR,ZCR,MUA,MUV,MUG,MWA,MWF,YAR,YFR)
0211          RHOG = 1. / (YAR/RHOA + YFR/RHOV)
0212          WRITE(1,1112)
0213    1112 FORMAT(" LAMBST,BM,BT,RHOFT,CPG,KG ")
0214          WRITE(1,*) LAMBST,BM,BT,RHOFT,CPG,KG
0215    C
0216    C
0217    C
0218    C   COMPUTE DROP HEAT-UP PARAMETERS
0219    C COMPUTE QUANTITIES WHICH DEPEND ON DROP SIZE
0220    C
0221      98  CONTINUE
0222    C
0223          DO 155 I=1,NDROP
0224          IF (TIME(I).LT.DELTAT) TSD(I) = FTEMP0
0225     100 IF ((TSD(I)-FTEMP0).GE.(0.95*(TSST-FTEMP0))) GOTO 3060
0226          TR = TSD(I) + (1./3.) * (TAI - TSD(I))
0227    C DENSITY OF AIR (KG/M**3)
0228          ZAIR = 1.0
0229    103   H = (0.003103/TR) * P / ZAIR
0230          ZAIRN = (1./(1.-H)) - (7349./TR**1.5) * (H/(1.+H))
0231          IF (ABS((ZAIRN-ZAIR)/ZAIRN).LT.0.0005) GOTO 105
0232          ZAIR = ZAIRN
0233          GOTO 103
0234    105   CONTINUE
0235          RHOA = MWA / ZAIR * (P/(8.314*TR))
0236    C   DENSITY OF FUEL VAPOR (KG/M**3)
0237          CALL VPRDN (TCR,PCR,MWF,TR,P,RHOV)
0238    C VISCOSITY OF AIR (KG/M*S) SUTHERLAND CORRELATION
```

```
0239          MUA = 1.425E-6 * SQRT(TR) /(1 + (100/TR))
0240    C  VISCOSITY OF THE FUEL VAPOR AND MIXTURE WITH AIR (KG/M*S)
0241          CALL VPRVS(TR,TCR,ZCR,MUA,MUV,MUG,MWA,MWF,YAR,YFR)
0242          TREDUC = TSD(I)/TCR
0243          A = 36/TREDUC - 35. - TREDUC**6 + 96.73*ALOG10(TREDUC)
0244          B = ALOG10(TREDUC) - 0.0364*A
0245          C = 7*ALOG10(TREDUC) - 0.118*A
0246          TERM1 = C - 1.192*B
0247          TERM2 = 4.93*B
0248          PREDUC = EXP(2.30259 * (TERM1 + ACENTR * TERM2))
0249          PFS = PREDUC * PCR
0250          PDIFF = P - PFS
0251          IF (PDIFF.LT.0.0) PDIFF = 0.0
0252          YFS = PFS*MWF / (PFS*MWF + PDIFF*MWA)
0253          YFR = YFS + (1./3.) * (YFI-YFS)
0254          YAR = 1. - YFR
0255          IF (TR.GT.600.) GO TO 3040
0256          CPA = 4.184 * (0.244388 - 4.20419E-5 * TR + 9.61128E-8 * TR**2
0257         & - 1.16383E-11 * TR**3)
0258          GO TO 3050
0259     3040 CPA = 4.184 * (0.208831 + 7.71027E-5 * TR - 8.56726E-9 * TR**2 -
0260         & 4.75772E-12 * TR**3)
0261     3050 CONTINUE
0262          CPV = (0.363 + 0.000467*TR) * (5. - 0.001*RHOF0)
0263          CPG = YAR * CPA + YFR * CPV
0264          IF (TR.GT.850.) GO TO 3100
0265          KA = 1.E-4 * (1.13841E-3 + 1.01789E-3*TR - 5.82577E-7*TR**2 +
0266         & 2.46855E-10*TR**3)
0267          GO TO 3110
0268     3100 KA = 1.E-4 * (-.0999992 + 1.19034E-3*TR - 5.29096E-7*TR**2 +
0269         & 1.11208E-10*TR**3)
0270     3110 CONTINUE
0271          E = 2.- 0.0372*(TR/TBN)**2
0272          KV = 1.E-6 * (13.2 - 0.0313 *(TBN-273.)) * (TR/273.)**E
0273          KG = YAR * KA + YFR * KV
0274          L = LTBN * ((TCR-TSD(I))/(TCR-TBN))**0.38
0275          BT = CPG * (TAI - TSST) / L
0276          BM = (YFS - YFI) / (1 - YFS)
0277          RHOG = 1. / (YAR/RHOA + YFR/RHOV)
0278          RHOFT = RHOF0*(1-1.8*CEX*(TSD(I)-288.6) - (0.090*(TSD(I)-288.6)**2
0279         & / (TCR - 288.6)**2))
0280          LAMBHU(I) = 8 * ALOG(1+BM) / (RHOFT * (CPG/KG))
0281    C PRANDTL NO.
0282     3060 PRNDT = CPG * MUG / KG
0283    C  REYNOLDS NO.
0284          RE(I) = D(I) * RHOG * SQRT((UP(I)-UA)**2 + (VP(I)-VA)**2 +
0285         & (WP(I)-WA)**2) / MUG
0286    C    MODIFY REYNOLDS NO. USED TO CALCULATE MASS LOSS TO INCLUDE A
0287    C    TERM FOR TURBULENCE INTENSITY EQUAL TO 20 PERCENT OF X-AXIS VEL
0288          REM(I) = D(I) * RHOG *(SQRT((UP(I)-UA)**2 + (VP(I)-VA)**2 +
0289         & (WP(I)-WA)**2) + 0.2*UA) / MUG
0290          IF ((TSD(I)-FTEMP0).GE.(0.95*(TSST-FTEMP0))) GOTO 3070
0291          LAMBA(I) = LAMBHU(I) * (1 + 0.276 * REM(I)**0.5 * PRNDT**0.33)
0292          GOTO 3080
0293     3070 CONTINUE
0294          LAMBA(I) = LAMBST * (1 + 0.276 * REM(I)**0.5 * PRNDT**0.33)
0295     3080 CONTINUE
0296          MASSD = (3.141596 / 6) * RHOFT * D(I)**3
0297          MDOT = (3.141596 / 4.) * RHOFT * LAMBA(I) * D(I)
0298          T = TSD(I) / TBN
```

```
0299          CPF =3.52390-6.15627*T+6.99895*T**2-2.47850*T**3+NOCARB*(-0.016019
0300         & -0.003128*T+0.172186*T**2-0.058406*T**3)
0301          TSD(I)=TSD(I)+(MDOT * L /(CPF * MASSD) * ((BT/BM) - 1.) * DELTAT)
0302          IF ((TSD(I)-FTEMP0).GE.(0.95*(TSST-FTEMP0))) TSD(I)=TSST
0303          D(I) = D(I) - (LAMBA(I)/(2.*D(I))) * DELTAT
0304          IF (D(I).LE.0.9E-6) D(I)=0.899E-6
0305    C DRAG COEFFICIENT, CD
0306          IF (RE(I).GT.80.) GO TO 110
0307          CD(I) = 27. * RE(I)**(-0.84)
0308          GO TO 130
0309     110  IF (RE(I).GT.10000) GO TO 120
0310          CD(I) = 0.271 * RE(I)**0.217
0311          GO TO 130
0312     120  CD(I) = 2.
0313     130  CONTINUE
0314    C DRAG FACTOR, F
0315          F(I) = 18. * MUG*CD(I) * RE(I) /(RHOFT * D(I)**2 * 24.)
0316    C NEW DROPLET VELOCITY AND POSITION
0317          UP(I) = -F(I) * (UP(I) - UA) * DELTAT + UP(I)
0318          VP(I) = -F(I) * VP(I) * DELTAT + VP(I)
0319          WP(I) = 0.
0320          XP(I) = UP(I) * DELTAT + XP(I)
0321          YP(I) = VP(I) * DELTAT + YP(I)
0322          ZP(I) = 0.
0323     150  CONTINUE
0324          IF (D(I).LE.0.9E-6) GO TO 152
0325          TIME(I) = TIME(I) + DELTAT
0326          GO TO 153
0327     152  D(I) = 0.9E-6
0328          KK = I
0329          GO TO 155
0330     153  CONTINUE
0331          IF (XP(I).LT.XPS) GO TO 100
0332     155  CONTINUE
0333    C
0334    C
0335    C
0336          DO 211 I = 1,NDROP
0337     211  DMU(I) = D(I) * 1.0E6
0338          GOTO 312
0339          DO 312 I=1,NDROP
0340          WRITE (6,310) I,TIME(I),DMU(I),XP(I),FF0(I)
0341     310  FORMAT (1X,I3,F10.5,F8.2,F8.2,F9.6)
0342     312  CONTINUE
0343    C COMPUTE ROSIN-RAMMLER PARAMETERS OF NEW DISTRIBUTION
0344          D(KK) = 0.9E-6
0345          D(0) = D(1)
0346          DIAM0(0) = DIAM0(1)
0347          UP(0) = UP(1)
0348          D(NDROP+1) = D(NDROP)
0349          DIAM0(NDROP+1) = DIAM0(NDROP)
0350          UP(NDROP+1) = UP(NDROP)
0351          SUMFF = 0.0
0352          DO 160 I=KK,NDROP
0353     160  SUMFF = SUMFF + FF0(I) *((D(I) / DIAM0(I))**3 / UP(I) + (D(I+1)
0354         & /DIAM0(I+1))**3 / UP(I+1))/2
0355          DO 170 I=KK,NDROP
0356     170  FF(I) = FF0(I) * ((D(I)/DIAM0(I))**3 / UP(I) + (D(I+1)/DIAM0(I+
0357         & 1))**3 / UP(I+1)) / 2 /SUMFF
0358          DO 175 I=KK,NDROP
```

```
0359   175  R(I) = 0.0
0360        DO 180 I=KK,NDROP
0361        DO 180 J=I,NDROP
0362   180  R(I) = R(I) + FF(J)
0363        K = NDROP
0364        DO 181 I=NDROP,KK+2,-1
0365   181  IF (R(I).LT.0.001) K = I-1
0366        KL = KK + 1
0367        DO 190 I=KL,K
0368        ZDATA(I) = ALOG(1/R(I))
0369        YDATA(I) = ALOG(ZDATA(I))
0370   190  XDATA(I) = ALOG(D(I))
0371        SUMX = 0.
0372        SUMY = 0.
0373        SUMX2 = 0.
0374        SUMY2 = 0.
0375        SUMXY = 0.
0376        DO 200 I=KL,K
0377        SUMX = SUMX + XDATA(I)
0378        SUMY = SUMY + YDATA(I)
0379        SUMXY = SUMXY + (XDATA(I) * YDATA(I))
0380        SUMX2 = SUMX2 + XDATA(I)**2
0381   200  SUMY2 = SUMY2 + YDATA(I)**2
0382        KD = K - KL + 1
0383        M = (SUMXY - (SUMX*SUMY/KD)) / (SUMX2 - (SUMX**2/KD))
0384        B = (SUMY - M * SUMX)/KD
0385        SIGMAX = SQRT((SUMX2 - (SUMX**2)/KD) / (KD-1))
0386        SIGMAY = SQRT((SUMY2 - (SUMY**2)/KD) / (KD-1))
0387        CC = M * SIGMAX / SIGMAY
0388        NNEW = M
0389        XBARNW = EXP(-B/NNEW)
0390        XBRNWM = XBARNW * 1.0E6
0391        IF (NNEW.LT.1.0) GOTO 202
0392        Y=2.-1./NNEW
0393        G = Y**Y*EXP(-Y)*SQRT(2.*3.1415/Y)*(1.+1./(12.*Y)+1./(288.*Y**2)
0394       & -139./(51840.*Y**3)-571./(2488320.*Y**4))
0395        SMD = XBRNWM * (1.-1./NNEW) / G
0396        GOTO 204
0397   202  WRITE(1,203)
0398   203  FORMAT (" VALUE OF N LESS THAN 1.0 ")
0399   204  CONTINUE
0400  C OUTPUT STATEMENTS
0401        WRITE (6,205)
0402   205  FORMAT (//,'  R-R XBAR (UM) ',' R-R N ',' CORR.COEF.',
0403       & '  SMD ')
0404        WRITE (6,210) XBRNWM,NNEW,CC,SMD
0405   210  FORMAT (F15.1,F15.2,F15.3,F15.2)
0406        WRITE (6,215)
0407   215  FORMAT (1X,/,7H   DIAM ,8H   TIME ,7H X DROP,7H Y DROP,7H Z DROP,
0408       C 8H   U-VEL,8H   V-VEL,8H   W-VEL,6H FTEMP,6H    RE)
0409        WRITE (6,220) (DMU(I),TIME(I),XP(I),YP(I),ZP(I),UP(I),VP(I),WP(I),
0410       C TSD(I),RE(I), I=1,NDROP)
0411   220  FORMAT (F7.1,F8.5,3F7.4,3F8.3,F6.1,F7.1)
0412    223 CONTINUE
0413        GOTO 2402
0414        WRITE (1,2400)
0415   2400 FORMAT(" LAMBHU(I), LAMBA(I), TSD(I) ")
0416        WRITE (1,2401) (LAMBHU(I),LAMBA(I),TSD(I), I=1,NDROP)
0417   2401 FORMAT (2E15.5,F15.3)
0418   2402 CONTINUE
```

```
      IF (XPS.LE.XPTT) GO TO 230
      GO TO 240
230   XPS = XPS + XPT
      GO TO 98
1099  WRITE(1,1098)
1098  FORMAT(" PROBLEM IN EVALUATING TSST AT ORIG LIMIT VALUES ")
      WRITE(1,*)LEFT,P,PFS,MWF,MWA,L,CPG,TAI,TS
240   CONTINUE
      STOP
      END
      SUBROUTINE VPRDN (TCR,PCR,MWF,TR,P,RHOV)
      REAL MWF
      R = 8.314
      A = 0.4276 * R**2 * TCR**2.5 / PCR
      B = 0.0867 * R * TCR / PCR
      BB = B / (R*TR)
      AB = A / (B*R*TR**1.5)
      Z = 1.0
2210  H = BB * P / Z
      ZN = (1./(1.-H)) - AB*(H/(1.+H))
      IF (((ZN-Z)/ZN).LT..0005) GO TO 2200
      Z = ZN
      GOTO 2210
2200  Z = ZN
      RHOV = (MWF/Z) * (P/(R*TR))
      RETURN
      END
      SUBROUTINE VPRVS (TR,TCR,ZCR,MUA,MUV,MUG,MWA,MWF,YAR,YFR)
      DIMENSION A(7)
      REAL MUA,MUV,MUG,MWA,MWF,OMEG,OMGINV
      EK = 65.3*TCR*ZCR**3.6
      SIG = 0.01866*(MWF/(RHOCR/1000.))**0.333 / ZCR**1.2
      A(1)=9.1426362E-1
      A(2)=-1.0689360
      A(3)=6.8077797E-1
      A(4)=-2.1208677E-1
      A(5)=3.4487186E-2
      A(6)=-2.8188225E-3
      A(7)=9.1590342E-5
      OMGINV = 0.
      DO 2300 I=1,7
2300  OMGINV = OMGINV + A(I)* (ALOG10(TR/EK))**I
      OMEG = 1./OMGINV
C  VISCOSITY OF FUEL VAPOR (PA*SEC  OR  KG/(M*SEC))
      MUV = 2.669E-8 *(MWF*TR)**0.5 / (SIG**2 * OMEG)
C  CALCULATE VISCOSITY OF MIXTURE
      PHI12=(1.+(MUA/MUV)**0.5*(MWV/MWA)**0.25)**2/(8.*(1.+MWA/MWV))**
     & 0.5
      PHI21=(1.+(MUV/MUA)**0.5*(MWA/MWV)**0.25)**2/(8.*(1.+MWV/MWA))**
     & 0.5
      MUG=MUA/(1.+PHI12*(YFR/MWF/(YAR/MWA))) + MUV/(1.+PHI21*(YAR/MWA/
     & (YFR/MWF)))
      RETURN
      END
```

## YEARLY DISTRIBUTION LIST

| No. of Copies | | No. of Copies | |
|---|---|---|---|
| 3 | Mr. Keith Ellingsworth<br>Mechanics Division<br>Material Sciences Division<br>Office of Naval Research<br>800 North Quincy Street<br>Arlington, VA 22217 | 6 | Technical Information Division<br>Naval Research Laboratories<br>4555 Overlook Ave. S.W.<br>Washington, DC 20375 |
| 1 | Mr. Dick Strucko<br>Code 2705<br>David Taylor Naval Ship R&D Center<br>Anapolis, MD 21402 | 12 | Defense Documentation Center<br>Bldg. 5<br>Cameron Station<br>Alexandriz, VA 22314 |
| 1 | Professor C.K. Law<br>Dept. of Mechanical Engineering &<br>Astronautical Sciences<br>Northwestern University<br>Evanston, IL 60201 | 1 | Professor F.L. Dryer<br>Mechanical and Aerospace<br>Engineering Dept.<br>Princeton University<br>Princeton, NJ 08544 |
| 1 | Mr. William Wagner<br>Naval Air Propulsion Center, PE-71<br>1440 Parkway Avenue<br>Trenton, NJ 08628 | 1 | Dr. A.M. Mellor<br>Department of Mechanical<br>Engineering & Mechanics<br>Drexel University<br>Philadelphia, PA 19104 |
| 1 | Mr. Andy Szaniszlo<br>Lewis Research Center<br>Propulsion Laboratory<br>21000 Brookpark Road<br>Cleveland, OH 44135 | 1 | Mr. John Marek<br>Lewis Research Center<br>Propulsion Laboratory<br>21000 Brookpark Road<br>Cleveland, OH 44135 |
| 1 | Mr. Bob Ingebo<br>Lewis Research Center<br>Propulsion Laboratory<br>21000 Brookpark Road<br>Cleveland, OH 44135 | 1 | Mr. Dan A. Grogan<br>05-R<br>CP6 R.802<br>Department of the Navy<br>Naval Sea Systems Command<br>Washington, DC 20362 |
| 1 | Mr. L.T. Yap<br>Mechanical & Aerospace Engineering Dept.<br>Princeton University<br>Princeton, NJ 08544 | 1 | Dr. C. Thomas Avedisian<br>Assistant Professor<br>Sibley School of Mechanical &<br>Aerospace Engineering<br>Upson & Grumman Halls<br>Cornell University<br>Ithaca, NY 14853 |
| | **LETTER OF TRANSMITTAL ONLY**<br>Defense Contract Administration Services<br>Management Area - San Antonio<br>P.O. Box 1040, Main Post Office<br>615 E. Houston St.<br>San Antonio, TX 78394 | 1 | Dr. Edward J. Mularz<br>Head, NASA Combustion<br>Fundamentals Section<br>Propulsion Laboratory<br>Research & Tech Laboratories<br>U.S. Army Aviation R&D Cmd.<br>Lewis Research Center<br>21000 Brookpark Road<br>Cleveland, OH 44135 |